



Water vapour and ozone in the upper troposphere – lower stratosphere: Global climatologies from three Canadian limb-viewing instruments

Paul S. Jeffery¹, Kaley A. Walker¹, Chris E. Sioris², Chris D. Boone³, Doug Degenstein⁴, Gloria L. Manney^{5,6}, C. Thomas McElroy⁷, Luis Millán⁸, David A. Plummer⁹, Niall J. Ryan¹, Patrick E. Sheese¹, and Jiansheng Zou¹

¹Department of Physics, University of Toronto, Toronto, ON, M5S 1A7, Canada

²Air Quality Research Division, Environment and Climate Change Canada, Toronto, ON, M3H 5T4, Canada

³Department of Chemistry, University of Waterloo, Waterloo, ON, N2L 3G1, Canada

⁴Department of Physics & Engineering Physics, University of Saskatchewan, Saskatoon, SK, S7N 5E2, Canada

⁵NorthWest Research Associates, Socorro, NM, 87801, USA

⁶Department of Physics, New Mexico Institute of Mining and Technology, Socorro, NM, 87801, USA

⁷Department of Earth and Space Science and Engineering, York University, Toronto, ON, M3J 1P3, Canada

⁸Jet Propulsion Laboratory, Pasadena, CA, 91109, USA

⁹Climate Research Branch, Environment and Climate Change Canada, Dorval, QC, H9P 1J3, Canada

Correspondence: Kaley A. Walker (kaley.walker@utoronto.ca)

Abstract. This study presents upper troposphere - lower stratosphere (UTLS) water vapour and ozone climatologies generated from 14 years (June 2004 to May 2018) of measurements made by three Canadian limb-viewing satellite instruments: the Atmospheric Chemistry Experiment - Fourier Transform Spectrometer (ACE-FTS), the Measurement of Aerosol Extinction in the Stratosphere and Troposphere Retrieved by Occultation (MAESTRO), and the Optical Spectrograph and InfraRed Imaging System (OSIRIS; ozone only). This selection of instruments was chosen to explore the capability of these Canadian instruments in representing the UTLS, and to enable analysis of the impact of different measurement sampling patterns. The water vapour and ozone climatologies have been constructed using tropopause-relative potential temperature and equivalent latitude coordinates in an effort to best represent the distribution of these two gases in the UTLS, which is characterized by a high degree of dynamic and geophysical variability. Zonal-mean multiyear-mean climatologies are provided with 5° equivalent latitude and 10 K potential temperature spacing, and have been constructed on a monthly, seasonal (3-month), and yearly basis. These climatologies are examined in-depth for two 3-month periods, December-January-February and June-July-August, and are compared to reference climatologies constructed from the Canadian Middle Atmosphere Model 39-year specified dynamics (CMAM39-SD) run, subsampled to the times and locations of the satellite measurements, in order to evaluate the consistency of water vapour and ozone between the datasets. Specifically, this method of using a subsampled model addresses the impact of each instrument's measuring pattern, and allows for the quantification of the influence of different measurement patterns on multiyear climatologies. In turn, this permits a consistent evaluation of the measurements of these two gas species. For the water vapour climatologies produced, a less than 8 % overall difference was found between the climatologies generated from the two versions of ACE-FTS, while comparisons with the MAESTRO climatologies were found to yield 15–41 % overall dif-



ferences, depending on the version of ACE-FTS and the season. When considering the ozone climatologies, those constructed from the two ACE-FTS versions agreed to within 2 % overall, and the OSIRIS ozone climatologies agreed with these to within 10 %. The MAESTRO ozone climatologies were found to differ from ACE-FTS and OSIRIS by about 30–35 % for the former, and 25 % for the latter, albeit with regions of better agreement within the UTLS. Overall these findings indicate that this set of Canadian limb sounders provide consistent water vapour and ozone distributions in the UTLS.

1 Introduction

Long-term observational and model-derived climatologies are widely used to represent the zonal-mean state of atmospheric constituents for a specific period as a function of altitude and geolocation coordinates. These climatologies provide information on the atmospheric environment and permit investigations into the distribution of trace gases and the patterns resulting from circulation and transport processes (e.g., Randel et al., 1998; Jones et al., 2012; Koo et al., 2017). Additional uses of climatologies include evaluating systematic differences between similarly composed model or observational datasets (e.g., Eckstein et al., 2017; Kolonjari et al., 2018), and acting as a priori information for the retrieval of trace gas profiles from observational measurements (e.g., Vigouroux et al., 2008; Sofieva et al., 2014). In recent years, there has been a push to expand the database of climatologies focused on one of the most challenging regions of the atmosphere to study, the upper troposphere - lower stratosphere (UTLS), in order to better constrain the role the UTLS plays in climate processes through detailed characterization of the constituents of the region (SPARC-CCMVal, 2010; SPARC-DI, 2017; Kunkel et al., 2018).

The UTLS is a crucial region of chemical, radiative, and dynamical activity in the atmosphere, spanning from approximately 300 hPa to 30 hPa (e.g., Holton et al., 1995; Gettelman et al., 2011). The tropopause, a dynamic barrier to transport that acts to separate the vertical transport regimes of the troposphere and stratosphere, strongly influences the chemical structure of the UTLS (Holton et al., 1995; Hoor et al., 2002; Pan et al., 2004). Stratosphere-troposphere exchange via localized processes, such as tropopause foldings, and components of the Brewer-Dobson circulation permit some chemical transport between the underlying and overlying regions, but overall the tropopause greatly restricts trace gas transport, giving rise to strong gradients in the horizontal and vertical (e.g., Holton et al., 1995; Roelofs and Lelieveld, 1997; Hoor et al., 2002; Pan et al., 2004; Hoor et al., 2010). Many of the mixing processes that do arise tend to be variable in nature, leading to rapidly-changing small-scale gas features that further impact the trace gas distributions around the UTLS (Holton et al., 1995; Roelofs and Lelieveld, 1997; Hoor et al., 2002; Pan et al., 2004; Hoor et al., 2010). The frequency of these localized mixing processes around the tropopause, along with the inherent variability of the tropopause layer itself, leads to the high degree of variability characteristic of the UTLS (Holton et al., 1995; Pan et al., 2004).

As a result of radiative effects arising from the thermal structure of the UTLS, knowledge of the distribution of trace gases within this region is critical in the development of an accurate understanding of climate forcing. Atmospheric temperatures are at a local minimum in the UTLS, which maximizes the influence that radiatively active gases have on atmospheric forcing (Forster and Shine, 2002; Gettelman et al., 2011; Riese et al., 2012). This holds for water vapour and ozone, two of the most important greenhouse gases, as both exhibit their greatest impact on surface temperature from their UTLS distributions where



their greenhouse gas efficiency is largest (Lacis et al., 1990; Forster and Shine, 1997; Solomon et al., 2010). Outside of their role as greenhouse gases, these two species collectively influence the chemical composition of the UTLS by providing ice surfaces for heterogeneous chemical reactions (water vapour; Brasseur and Solomon, 2005), producing hydroxyl radicals that rapidly react with other gases (water vapour; Brasseur and Solomon, 2005), and by absorbing ultraviolet and infrared light to moderate the energy balance of the UTLS (ozone; Lacis et al., 1990). Water vapour is primarily concentrated near the ground, with a strong negative gradient extending upwards to the tropopause, while ozone is mainly concentrated in the stratosphere, with a gradient extending away from its maximum concentration in the tropical middle stratosphere. The limited stratospheric water vapour arises mainly from upwards transport at the equator, though these air parcels are largely dehydrated when passing through the low-temperature tropical tropopause region, with the oxidation of methane serving as a secondary source (Holton et al., 1995; Brasseur and Solomon, 2005). In the free troposphere, ozone is enhanced by stratosphere-troposphere processes that move air parcels rich in ozone down into the troposphere, including the seasonally-varying Brewer-Dobson circulation (Roelofs and Lelieveld, 1997; Lelieveld and Dentener, 2000; Pan et al., 2004).

Despite the large impact the UTLS has on climate, it remains one of the least well characterized regions of the atmosphere because of the challenging measurement conditions posed by the region. Included in this are the relatively low chemical concentrations of many of the trace gas constituents compared to their concentrations elsewhere in the troposphere or stratosphere, the presence of clouds that can inhibit remote observations over widely employed measurement frequencies, and the frequent localized mixing processes around the tropopause, which, along with the inherent variability of the tropopause layer itself, leads to the high degree of variability characteristic of the UTLS (Holton et al., 1995; Pan et al., 2004). Many UTLS-focused studies of water vapour and ozone have employed aircraft and balloon-borne instruments, including ozonesondes and radiosondes, to make highly vertically resolved measurements of trace gases (e.g., Kunz et al., 2011; Hurst et al., 2011; Zahn et al., 2014; Eckstein et al., 2017). The detail provided by these measurements facilitates process studies; however analysis of temporal and spatial variations is restricted as measurements are often regionally-focused, performed as part of discontinuous measurement campaigns, or both (Kunz et al., 2008; Zahn et al., 2014). Detailed analysis of UTLS composition, including long-term trends in trace gases, requires decadal global observational datasets, which satellite instruments are capable of providing (e.g., Hegglin et al., 2010, 2021). Chemistry-climate models can aid investigations into climate forcings, such as greenhouse gases, by providing detailed simulations of chemical and transport processes; however these must be characterized against measurements to ensure their veracity (e.g., Pendlebury et al., 2015; Kolonjari et al., 2018).

The need for well characterized trace gas climatologies that can serve toward the parallel goals of analyzing gas distributions and trends, and of validating model datasets, is emphasized in the reports produced as a part of the Stratosphere-troposphere Processes And their Role in Climate (SPARC) Chemistry-Climate Model Validation (SPARC-CCMVal, 2010) and the SPARC Data Initiative (SPARC-DI, 2017) projects. Key recommendations for future work from this latter activity highlighted the need to study the UTLS in greater detail to address outstanding questions concerning the behaviour of trace gases (SPARC-DI, 2017). Specifically, the climatologies analyzed in the SPARC Data Initiative included the UTLS, but emphasis was on the stratosphere as a whole and only a small subset of associated activities (e.g., Neu et al., 2014), focused on the UTLS in particular. To fully



characterize the differences between instruments in the UTLS, this report stressed the need for climatologies to be constructed in ways to best minimize the effects of geophysical variability on the diagnostics compared (SPARC-DI, 2017).

In recent years, many major activities and individual studies have considered water vapour and ozone as measured by a variety of satellite instruments. Included in this list of activities is the SPARC Water Vapour Assessment 2 (WAVAS II), the SPARC Long-term Ozone Trends and Uncertainties in the Stratosphere (LOTUS), the Stratospheric Water and Ozone Satellite Homogenized (SWOOSH) climate data record, and the European Space Agency's Water Vapour Climate Change Initiative (Water_Vapor_CCI) and Ozone Climate Change Initiative (Ozone_CCI), with some projects employing well over a dozen instrument datasets (e.g., Davis et al., 2016; Lossow et al., 2019; SPARC-LOTUS, 2019; Hegglin et al., 2021). While many of these activities have a UTLS component, the majority of recent studies are not focused on climatologies, or in cases where they are, these are not made with a focus on the UTLS, such as the recent update to the SPARC Data Initiative (Hegglin et al., 2021). One of the driving principles of the ongoing SPARC Observed Composition Trends And Variability in the Upper Troposphere and Lower Stratosphere (OCTAV-UTLS) activity is to address the need for UTLS-focused climatologies, produced with an aim to minimize the effects of geophysical variability by accounting for geophysical conditions (Kunkel et al., 2018). Additionally, this activity aims to address the influence of disparate sampling patterns in this region to maximize the use of available datasets. As reported by Toohey and von Clarmann (2013) and Millán et al. (2016), nonuniform sampling by instruments due to their measurement patterns can introduce significant systematic errors when comparing datasets, which is not accounted for in many comparison studies of climatologies. Toohey et al. (2013), as part of the SPARC Data Initiative, found that sampling biases can lead some measurement climatologies to possess water vapour differences in excess of 10 % and differences in ozone exceeding 20 % around the UTLS, emphasizing the need to constrain this error in future climatology comparisons.

With this in mind, the aim of this study is to produce, analyze, and compare zonal-mean multiyear-mean water vapour and ozone climatologies that utilize data from three Canadian limb-viewing satellite instruments, the Atmospheric Chemistry Experiment - Fourier Transform Spectrometer (ACE-FTS), the Measurement of Aerosol Extinction in the Stratosphere and Troposphere Retrieved by Occultation (MAESTRO), and the Optical Spectrograph and InfraRed Imaging System (OSIRIS; ozone only), in support of the OCTAV-UTLS activity. All three instruments measure into the UTLS with high vertical resolution, have long data records, and provide global coverage over the course of the year, making them good fits to study this highly variable region (Bernath et al., 2005; McElroy et al., 2007; Haley et al., 2004, respectively). While these instruments have been employed in previous climatology studies (e.g., Neu et al., 2014; SPARC-DI, 2017; Hegglin et al., 2021), the climatologies produced here employ tropopause-referenced vertical coordinates, which have been shown capable of reducing the effects of geophysical variability by parcelling the data based on the processes which drive this variability, thereby ensuring only similarly driven data are assessed or compared (e.g., Pan et al., 2004; Hoor et al., 2004; Hegglin et al., 2008; Manney et al., 2011). Specifically, tropopause-referenced potential temperature is employed because of its ability to account for the role of the tropopause as a transport barrier, which enables it to represent the large trace gas gradients that arise around the tropopause leading to improved partitioning of data (e.g., Pan et al., 2004; Manney et al., 2011). The meridional coordinate employed in these climatologies is potential vorticity derived equivalent latitude, which has been shown capable of grouping air masses based on dynamical conditions, thereby reducing the effect of sporadic meridional transport in the UTLS (e.g., Hoor



et al., 2004; Hegglin et al., 2006). However, this coordinate possesses limitations, such as in representing tropospheric transport processes, as shown in Manney et al. (2011) and Pan et al. (2012). In spite of these limitations, through the combination of these coordinates the inherent variability of the UTLS can be well constrained in the resulting climatologies.

The climatologies presented here cover the 14-year period between 1 June 2004 and 31 May 2018, and are intended to both
125 provide a well characterized representation of water vapour and ozone as measured by the three instruments involved in this study, and to provide a source of data for future work including intercomparison studies and model validation. To characterize the differences between the datasets, the CMAM39-SD model output dataset is employed to serve as a consistent comparison reference. Adapting the methods of Kolonjari et al. (2018), the model is sampled at the times and locations of the instrument measurements, in order to generate subsampled model climatologies of ozone and water vapour, which permits the sampling-
130 related differences between the datasets to be explored free from the influence of any retrieval biases between the instruments. In addition to the multiyear-mean climatologies, these equivalent-latitude zonal-mean climatologies are also produced on a monthly basis for the same 14-year period; detailed examination of which is outside of the scope of this study.

The rest of the paper is organized as follows; Sect. 2 addresses the satellite and model simulation datasets used, along with the means by which the tropopause height and equivalent latitude are determined for the datasets. Section 3 addresses the method
135 used to generate water vapour and ozone climatologies, as well as the approach taken to comparing these climatologies using a set of subsampled model climatologies. Sections 4 and 5 explore the resulting climatologies of water vapour and ozone, along with an intercomparison between the climatologies for each gas generated from each dataset. Finally, a summary is presented in Sect. 6.

2 Datasets

140 This section outlines the datasets used in this study. Sections 2.1 through 2.3 cover the satellite instruments used, one of which contributes two data versions to this study, while Sect. 2.4 addresses the reanalysis products that provide auxiliary data about atmospheric conditions for these measurement products. Section 2.5 describes the model output employed in this study.

2.1 ACE-FTS

The Canadian satellite SCISAT-1 was launched into a circular low-Earth orbit (650 km altitude, 74° inclination) on 12 August
145 2003 (Bernath et al., 2005). A primary objective of the Atmospheric Chemistry Experiment (ACE) mission aboard SCISAT-1 is to study chemical and dynamical processes impacting ozone distributions in the upper troposphere and stratosphere, using the solar occultation measurement technique (Bernath et al., 2005). Scientific operations of the ACE instruments commenced February 2004, and are ongoing.

A Fourier transform spectrometer, ACE-FTS, makes measurements covering the spectral range 750–4400 cm⁻¹ with 0.02 cm⁻¹
150 spectral resolution (Bernath et al., 2005; Boone et al., 2005, 2013, 2020). Operating in a limb-viewing geometry, ACE-FTS records absorption spectra twice per orbit, corresponding to sunrise and sunset occultations as seen by the instrument. Measurements are made at tangent heights spanning from the cloud tops to 150 km, with vertical spacing between 1.5 and 6 km



and a vertical field-of-view of 3–4 km (Bernath et al., 2005). In the UTLS, the vertical resolution of ACE-FTS combined with oversampling throughout the region leads to an effective resolution of about 1 km, making it ideal for studying gases in this region (Hegglin et al., 2008; Kolonjari et al., 2018). Under typical conditions, up to 15 sunrise and 15 sunset measurements can be made per day. Over the course of the year the latitudinal coverage of ACE-FTS spans from 85°N to 85°S, with a focus on the polar regions; however, due to the orbital inclination of SCISAT-1, it takes approximately three months to cover this range (Bernath, 2017).

Vertical profile information about temperature, pressure, and concentration as volume mixing ratio (VMR) for several dozen trace gas species comes from inversions of the solar occultation measurements made by ACE-FTS. The retrieval process is described fully in Boone et al. (2005, 2013, 2020), but in brief it begins with a CO₂ analysis through which pressure and temperature profiles are established. Using these temperature and pressure profiles, a global Levenberg-Marquardt nonlinear least square fitting algorithm is applied to the measured spectra to yield VMR profiles for the desired gas species. As part of the retrieval, the profiles are made available on a uniform 1-km grid (Boone et al., 2005, 2013).

In this work both version 3.6 (v3.6) and version 4.2 (v4.2) profiles of water vapour and ozone are used. While v3.6 (and its predecessor version 3.5, which uses an identical algorithm but in a different computational environment) ozone and water vapour profiles have been extensively validated and studied (e.g., Sheese et al., 2017; Bogner et al., 2019; Lossow et al., 2019), v4.2 is still undergoing validation (e.g., Sheese et al., 2022). As described in Boone et al. (2020), the key difference between these versions is that v4.2 retrievals use a CO₂ input for the temperature and pressure retrievals that explicitly accounts for seasonal and latitudinal variations and has an improved rate of change compared to the v3.6 CO₂ input, as well as consideration for the age of air in the stratospheric distribution of CO₂. Additionally, CO₂ is retrieved below 18 km in v4.2, necessitating that temperature and pressure information below this altitude are obtained from operational outputs from a global weather assimilation and forecasting system. A consequence of retrieving CO₂ is that in the v4.2 retrieval, the instrument pointing information is determined through analysis of the N₂ continuum, as opposed to analysis of CO₂ lines as done in the v3.6 retrieval (Boone et al., 2020). A set of quality control flags has been developed for the ACE-FTS v3.6 and v4.2 products (Sheese et al., 2015). These have been applied to the ACE-FTS data used in this work to filter extreme outliers from the data, with all profiles flagged with values between 4 and 7 being removed as recommended in Sheese et al. (2015). This method was found to reject 3.0 % of v3.6 H₂O, 1.8 % of v3.6 O₃, 1.6 % of v4.2 H₂O, and 1.0 % of v4.2 O₃ profiles used in this study. ACE-FTS data products have been used previously for a variety of applications, including climatology development (e.g., Jones et al., 2012; Koo et al., 2017; SPARC-DI, 2017; Hegglin et al., 2021), trend analysis (e.g., Fernando et al., 2020), and model studies and validation (e.g., Pendlebury et al., 2015; Kolonjari et al., 2018).

Recent work by Sheese et al. (2022) found that one of the key impacts to the trace gas products from the change from ACE-FTS v3.6 to v4.2, is that the newer product corrects a systematic drift in the former. Specifically, in comparing coincident measurements of ozone from ACE-FTS v3.6 and v4.2 against an ensemble of five different instruments, the ACE-FTS v3.6 product was found to experience a significant drift of $-1.0 \pm 0.4 \text{ \% dec}^{-1}$ between 20 and 35 km, whereas no drift of any significance was detected in the ACE-FTS v4.2 product (Sheese et al., 2022). The observed drift in the ACE-FTS v3.6 ozone



product arose from inaccurate CO₂ modeling, which would likewise impact the v3.6 water vapour product (Sheese et al., 2022). Below 21 km, Sheese et al. (2022) found that neither ACE-FTS version displayed a significant drift.

Global coincident measurement comparisons by Sheese et al. (2017) showed that ACE-FTS v3.5 water vapour concentrations are about 5 % lower than those measured by the Michelson Interferometer for Passive Atmospheric Sounding (MIPAS) and 5–20 % lower than the Aura – Microwave Limb Sounder (Aura-MLS) measurements in the lower stratosphere. In the upper troposphere, the bias with MIPAS is between -5 and +15 % and Aura-MLS yields larger concentrations of water vapour, in particular near the lower bound of sensitivity where the difference exceeds 50 %. Further comparisons of the ACE-FTS v3.5 water vapour dataset by Lossow et al. (2019) against an ensemble of coincident global satellite instruments indicated that ACE-FTS v3.5 water vapour in the lower stratosphere is about 3–8 % drier than other measurements, while in the upper troposphere ACE-FTS is drier by approximately 10–40 %. However, comparisons with the Stratospheric Aerosol and Gas Experiment III instrument on the International Space Station (SAGE III/ISS) by Davis et al. (2021) showed a wet bias for ACE-FTS v3.6 exceeding 20 % in the upper troposphere, and at about 5 % in the lower stratosphere, indicating a dependence of the bias on the comparison instrument. Comparisons of coincident measurements made by ACE-FTS v3.6 against the Polar Environment Atmospheric Research Laboratory Fourier Transform InfraRed spectrometer (PEARL FTIR) in the Canadian high Arctic indicated that ACE-FTS has a wet bias compared to this instrument of 7–10 % in the UTLS. Further comparisons against in-situ radiosondes contrasted this by yielding a slight dry bias in ACE-FTS v3.6, of about 0–9 %, in the upper troposphere, and a slight wet bias, of less than 2 %, in the lower stratosphere (Weaver et al., 2019).

Sheese et al. (2017) also examined ACE-FTS v3.5 ozone, and found it to be within ± 5 % of both Aura-MLS and MIPAS in the lower stratosphere, while in the upper troposphere these differences reached as high as 30 % for MIPAS and 40 % for Aura-MLS, with ACE-FTS biased low at these lower altitudes. McCormick et al. (2020) compared the v3.6 ozone profiles to SAGE III/ISS and found similar agreement, to within ± 5 %, as did Sheese et al. (2017) over the lower stratosphere. Bogner et al. (2019) found ACE-FTS v3.6 ozone over the high Arctic to be about 5 % larger in the upper troposphere and 5 % smaller in the lower stratosphere, than OSIRIS, and between 5 and 10 % larger than MAESTRO over the UTLS. In addition to their work in evaluating the drift in the ACE-FTS products, Sheese et al. (2022) also determined that ACE-FTS v3.6 ozone is biased high by 3–5 % between 15 and 25 km, while the ACE-FTS v4.2 ozone bias ranged from -1 % to +5 % over this same altitude range, as determined from a weighted comparison to MAESTRO, OSIRIS, the Sounding of the Atmosphere using Broadband Emission Radiometry (SABER) instrument on the NASA TIMED satellite, Aura-MLS, and the Odin Sub-Millimetre Radiometer (Odin-SMR).

Climatologies have also been compared as done in Hegglin et al. (2021), the update to the SPARC-DI (2017), which compared water vapour and ozone climatologies to multi-instrument mean climatologies. They found ACE-FTS v3.6 has a high bias for ozone in the upper troposphere by about 10–20 % that transitions to a roughly 3–5 % high bias in the lower stratosphere, with an exception for the southern polar region which is biased low by about 20 %. ACE-FTS v3.6 water vapour was found to be biased high over the upper troposphere by 20–50 %, and generally biased low in the lower stratosphere, by 0–10 %, with an exception for the southern polar region where differences can approach 50 % (Hegglin et al., 2021). These findings agree with recent work for ACE-FTS water vapour (Lossow et al., 2019), as do the lower stratospheric differences for ozone



(Sheese et al., 2022), but some disagreement is noted between climatological and profile comparisons in the upper troposphere for ozone. Part of this discrepancy is the result of non-uniform temporal sampling of ACE-FTS, which can lead to larger biases when comparing climatologies than when comparing coincident profiles between datasets, due to variations in trace gas distributions over time. This holds for climatological comparisons made with other measurement datasets and spurs the use of model-subsampled comparisons in this work.

2.2 ACE-MAESTRO

The second instrument aboard SCISAT-1 is MAESTRO, a dual spectrograph designed to measure between 285 and 1030 Nm, with the two grating spectrophotometers recording spectra with a wavelength dependent resolution of 1–2 Nm (McElroy et al., 2007). MAESTRO operates in a limb-viewing solar occultation mode, sharing the same suntracker and optical bore as ACE-FTS, making measurements during sunrise and sunset. One measurement sequence consists of 60 spectra taken between the cloud tops and 100 km above the ground, as well as 20 spectra taken between 100 km and 150 km for use as reference spectra. Measurements are made with a vertical resolution of 1–2 km (McElroy et al., 2007). Over time, MAESTRO has been affected by the gradual buildup of an unknown contaminant, and since 2015 no light with wavelength shorter than 500 Nm is transmitted through the instrument; however the water vapour and ozone retrievals remain operational (Sioris et al., 2016; Bernath, 2017).

Currently measurements made by MAESTRO are used to retrieve profiles of ozone, water vapour, aerosols, and optical depth. Herein we use the MAESTRO version 3.13 (v3.13) ozone and version 31 (v31) water vapour products. The ozone retrieval is detailed in McElroy et al. (2007) and Bognar et al. (2019), and the water vapour retrieval is described in detail in Sioris et al. (2010, 2016). Both inversions use the ACE-FTS v3.6 pressure and temperature profiles, so profiles can only be retrieved when there is a successful coincident ACE-FTS retrieval. This reliance on the ACE-FTS v3.6 pressure and temperature does however introduce the possibility of a drift in the MAESTRO products because of the systematic CO₂ modeling error discussed above and in Sheese et al. (2022). The ozone retrievals are based on a two-step approach wherein a modified differential optical absorption spectroscopy technique is used to obtain line-of-sight slant column densities at each measurement tangent height, which are then used to derive vertical profiles of ozone VMR using a nonlinear Chahine relaxation inversion (McElroy et al., 2007; Kar et al., 2007; Bognar et al., 2019). The water vapour retrieval uses a variation of this technique, with VMR profiles retrieved directly from a Chahine relaxation inversion of the observed differential optical depth rather than from derived slant column amounts (Sioris et al., 2010, 2016). This technique relies upon using the retrieved MAESTRO ozone profile as input for the inversion. MAESTRO water vapour is primarily a tropospheric product, as an upper altitude limit of approximately 17–22 km is imposed, stemming from the lower detection limit for spectrally averaged differential optical depth (Sioris et al., 2010, 2016). The altitude of this limit varies with the water vapour content in the lower stratosphere, with drier conditions leading to a lower upper altitude limit. MAESTRO ozone and water vapour products have been used in prior studies for purposes including climatology comparisons (e.g., SPARC-DI, 2017; Hegglin et al., 2021), drift analysis (e.g., Hubert et al., 2016; Lossow et al., 2019), and analysis of dynamical variability (Sioris et al., 2016).

A set of quality control flags has been calculated for the MAESTRO v3.13 ozone and v31 water vapour products following the method of Sheese et al. (2015). These were applied to the MAESTRO data used in this work, and all profiles flagged



with values between 4 and 7 were removed from the water vapour dataset as recommended in Sheese et al. (2015), while all profiles with nonzero flags were removed from the ozone dataset (personal communication with P. Sheese, 16 December 2019). This method was found to reject 2.5 % of v31 H₂O and 8.9 % of v3.13 O₃ profiles. Despite a large number of ozone profiles being removed, large variability is still observed in the MAESTRO ozone product, as will be discussed in Sect. 5.1. This is
260 influenced by the conflict between the underlying philosophy of the quality flags, which prioritizes retaining all potentially valid measurements, and the extremely high variability of the MAESTRO ozone product. A consequence of this is that it is not possible to reliably identify all outliers in the MAESTRO ozone dataset using these quality flags.

Bognar et al. (2019) compared profiles from OSIRIS, ACE-FTS, and MAESTRO over the Canadian high Arctic and found MAESTRO v3.13 ozone concentrations to be about 10 % smaller than data from the other two instruments in the lower strato-
265 sphere. This low bias is further reflected in climatological studies involving MAESTRO ozone, such as Hegglin et al. (2021), who found low biases of around 50 % in the upper troposphere and 10–20 % in the lower stratosphere, except for the tropics where it had a high bias of about 20 % compared to a multi-instrument mean ozone climatology. In terms of water vapour, Weaver et al. (2019) found that the previous version of MAESTRO water vapour, v30, was biased low by 6–12 % in the upper troposphere, and by less than 2 % in the lower stratosphere as compared to measurements from the PEARL FTIR. As compared
270 to radiosondes, MAESTRO had a mean upper tropospheric bias between 16 and 64 %, but a lower stratosphere bias of less than 3 % (Weaver et al., 2019). The global comparisons of MAESTRO v31 water vapour against an ensemble of instruments, as performed by Lossow et al. (2019), indicate that the MAESTRO bias is roughly parabolic with altitude. Specifically, around the tropopause there is an approximately 10 % dry bias, while into the troposphere and lower stratosphere this bias flips, approaching a 50 % wet bias (Lossow et al., 2019). The exception to this is for MAESTRO measurements in the tropics, which
275 are generally biased high by about 25 % over the entire UTLS. Climatologies constructed from the MAESTRO v31 water vapour are compared in Hegglin et al. (2021), where they show a generally positive bias, by 20–50 %, with regions of negative bias in the southern polar region, southern midlatitudes, and the northern polar region, with differences of about 50 %.

2.3 Odin-OSIRIS

The Odin satellite was launched 20 February 2001 into a near-circular Sun-synchronous low Earth (600 km) orbit at 98°
280 inclination (Murtagh et al., 2002). The ascending (descending) node of Odin was originally at 18:00 (6:00) local time, but a slight procession in its orbit has shifted this over time to an hour later, and subsequently back to only half an hour later than its original time (Llewellyn et al., 2004; Bourassa et al., 2014). Odin was designed for a mixed aeronomy/astronomy mission, with the aeronomy objective of studying anthropogenically-derived atmospheric changes with a focus on ozone-related science in the middle atmosphere (Murtagh et al., 2002). Routine operation of Odin began in November 2001 and continues through
285 to the present. Focus was split between the aeronomy and astronomy observation modes, with daily changeover between the two, until May 2007, after which Odin has made solely atmospheric observations.

OSIRIS is one of two aeronomy instruments aboard Odin. It consists of a grating optical spectrograph (OS) that records Rayleigh- and Mie-scattered sunlight spectra from 280–810 nm with 1–2 nm resolution, and an infrared imager (IRI) measuring airglow (Llewellyn et al., 2004). Operating in a limb-viewing geometry, OSIRIS is swept through tangent heights spanning



290 from 7 km to 70 km under its typical operation mode, with 30–60 of these vertical scans taken every orbit, and one orbit
completed every 96 minutes (Haley et al., 2004). The measured limb-radiance profiles have an altitude-dependant vertical
resolution of 1–2 km, with approximately 1 km vertical resolution near the tropopause (Haley et al., 2004). A result of Odin’s
orbital geometry relative to the position of the illuminated portion of the planet is that coverage focuses on the southern hemi-
sphere between October and February and the northern hemisphere between March and September. In October and February,
295 near global coverage, from 82° N to 82° S, is attained (Haley et al., 2004).

Ozone profiles are retrieved using the SaskMART algorithm described in detail in Degenstein et al. (2009). This algorithm
is an iterative Multiplicative Algebraic Reconstruction Technique (MART) that uses limb radiance spectra to retrieve ozone
number density profiles from the cloud tops to 60 km. The inversion requires aerosol and nitrogen dioxide profiles, pre-retrieved
from the same OSIRIS data, as well as temperature and air density profiles from the European Centre for Medium-Range
300 Weather Forecasts (ECMWF) ERA-Interim reanalysis (Bourassa et al., 2018). The version 5.10 (v5.10) OSIRIS ozone data
are used in this study, in which a pointing error that affected data above 20 km in the previous version 5.07 product has been
corrected (Bourassa et al., 2018). The reported ozone number density values are converted into VMRs using the ERA-Interim
reanalysis temperature and pressure information used in the retrievals. OSIRIS ozone products have been used in a variety
of prior studies, including climatology development (e.g., SPARC-DI, 2017; Hegglin et al., 2021), trend analysis (e.g., Sioris
305 et al., 2014; Bourassa et al., 2014; SPARC-LOTUS, 2019), and model evaluation (e.g., Pendlebury et al., 2015).

Adams et al. (2013) found that the previous OSIRIS ozone product, v5.07, is within $\pm 5\%$ of SAGE II satellite measurements,
and similar results were found by Adams et al. (2014) when comparing the same product to ozonesondes. However, this latter
study found that this ozone product is generally biased low by about 10 % in the lower stratosphere, and biased high in the
upper troposphere by up to 20 %, as compared to Aura-MLS. Further analysis of the v5.07 product by Hubert et al. (2016)
310 found low biases of 5–10 % in the UTLS outside of the tropics, and a larger low bias in the tropics of more than 15 % when
compared to coincident ground-based ozonesonde and lidar measurements. Bourassa et al. (2018) noted that the v5.07 OSIRIS
ozone product was subject to a gradual drift, but comparisons of this and the corrected v5.10 product indicated that this drift
was only significant above 20 km, so the v5.07 UTLS comparisons should be generally comparable to what would be found
for the v5.10 data used in this work. Comparisons by Bognar et al. (2019) in the Canadian high Arctic found that OSIRIS
315 v5.10 ozone is within $\pm 5\%$ of the v3.6 ACE-FTS ozone, and about 10 % larger than MAESTRO over the lower stratosphere.
Finally, climatology comparisons by Hegglin et al. (2021) found the v5.10 ozone product to be biased low compared to the
multi-instrument mean by about 10–20 % in the UTLS, except for a region of high bias in the tropical upper troposphere where
it displayed ozone values approximately 20 % larger than the mean.

2.4 JETPAC

320 Analysis of these satellite measurement products requires additional information concerning dynamical conditions of the at-
mosphere that must be derived from meteorological reanalyses (Manney et al., 2007). These properties include potential vor-
ticity, wind speeds, and tropopause locations, which enable the characterization of atmospheric transport. In this study, aux-
iliary data products for the satellite datasets come from the JEt and Tropopause Products for Analysis and Characterization



(JETPAC) software package, described in Manney et al. (2011, 2014, 2017) and Manney and Hegglin (2018). The JETPAC
325 algorithms identify and characterize atmospheric features and fields from reanalysis datasets, including three products rele-
vant to this study; tropopause location, equivalent latitude, and potential temperature. For tropopause properties, dynamical
tropopauses are identified using potential vorticity isopleths with values ranging between 1.5 potential vorticity units (PVU,
1 PVU = 10^{-6} K m² kg⁻¹ s⁻¹) and 6.0 PVU with an upper constraint provided in the tropics by the 380 K potential tempera-
ture contour (Manney et al., 2011). As many as four tropopauses can be identified for each of the tropopause definitions during
330 each reanalysis timestep and, once identified, location information, including altitude, potential temperature, and pressure, is
determined for each. The potential temperature is calculated from air temperature and pressure, and equivalent latitude is de-
termined by mapping the potential vorticity (PV) of an isentrope to a latitude field using the area enclosed by the PV isopleths
on this surface (Butchart and Remsburg, 1986).

The JETPAC products used here are derived from the Modern-Era Retrospective Analysis for Research and Applications,
335 version 2 (MERRA-2) reanalysis dataset, which is described in Gelaro et al. (2017). MERRA-2 is an atmospheric reanalysis
produced using the Godard Earth Observation System (GEOS) version 5.12.4 atmospheric data assimilation system, which
in turn uses the GEOS atmospheric model and the Gridpoint Statistical Interpolation analysis three-dimensional variational
(3DVAR) scheme (Gelaro et al., 2017, and the references therein). The reanalysis is provided at 0.5° by 0.625° resolution,
the same spatial resolution as the GEOS model, with 72 vertical levels spanning from the surface to 0.01 hPa (Gelaro et al.,
340 2017). The JETPAC products have been calculated at the locations and times of each measurement made in the ACE-FTS v3.6,
ACE-FTS v4.2, and OSIRIS v5.10 datasets. The geolocation information for the ACE-FTS datasets covers the entire profile,
while for OSIRIS only the position of the tangent point of one measurement altitude is available, at approximately 35 km above
the surface, and so this position is assumed for the entire OSIRIS profile. All MAESTRO profiles need an associated successful
ACE-FTS retrieval to provide temperature and pressure information and current versions of the MAESTRO products use the
345 ACE-FTS v3.6 information for these fields. Therefore the JETPAC product produced for ACE-FTS v3.6 has also been used for
the MAESTRO datasets.

2.5 CMAM39-SD

The free running extension of the Canadian Centre for Climate Modeling and Analysis (CCCma) third-generation atmospheric
general circulation model (AGCM3) is the Canadian Middle Atmosphere Model (CMAM), which uses AGCM3 as the un-
350 derlying basis for its middle atmosphere dynamical and chemistry-climate modelling components (de Grandpré et al., 2000;
Scinocca et al., 2008). The photochemistry component of CMAM incorporates fields for several dozen trace gases, with no-
table species including water vapour, methane, ozone, and species related to catalytic ozone loss (de Grandpré et al., 2000;
Jonsson et al., 2004). CMAM39-SD is the nudged specified dynamics run of CMAM that aims to estimate the chemical and
dynamical state of the atmosphere between 1980 and 2018. Free running models are incapable of reproducing day-to-day vari-
355 ations in meteorology, which hinders direct comparisons between observed and simulated trace gas concentrations, because
of the inherently chaotic nature of atmospheric circulation (McLandress et al., 2014). To address this deficiency, Newtonian
relaxation, known as nudging, can be applied to constrain temperature and circulation fields to a reanalysis dataset. This min-



360 imizes the internal variability of the model's circulation and allows for more direct comparisons (McLandress et al., 2014; Shepherd et al., 2014). The nudging for CMAM39-SD is implemented by relaxing the horizontal wind fields and temperature to the ERA-Interim reanalysis for the 1980 to 2018 period, with nudging applied at large spatial scales ($<T21$) from the surface to 1 hPa with a relaxation time constant of 24 hours (McLandress et al., 2014). The temperature fields from the ERA-Interim reanalysis at and above 5 hPa are adjusted to remove discontinuities in the system (McLandress et al., 2014). Prior nudged specified dynamics runs of CMAM, such as CMAM30-SD, which focused on the 1980 to 2010 period, have been found to agree well with Aura-MLS observations of meteorological fields (McLandress et al., 2013).

365 For CMAM39-SD, CMAM was run at 3.75° by 3.75° (T47) resolution, with 71 hybrid-sigma vertical pressure coordinate levels extending to approximately 95 km (Scinocca et al., 2008). The vertical resolution, which varies with altitude, increases with altitude from approximately 900 m at 300 hPa to 1500 m at 30 hPa (Scinocca et al., 2008). Fields from CMAM39-SD are sampled every 6 hours, starting at midnight, and are provided on their native hybrid-sigma pressure coordinate grid. This vertical grid is converted into pressure using prescribed atmospheric pressure changes and the model surface pressure. In contrast to the satellite datasets, the potential temperature, equivalent latitude, and tropopause locations for CMAM39-SD are calculated from the simulation fields directly. Modified versions of the JETPAC algorithms are used for these fields for consistency, and hence these products are referred to as JETPAC-like in this study. Prior comparisons of the CMAM30-SD water vapour and ozone simulations have found good agreement in the stratosphere with satellite datasets (e.g., Pendlebury et al., 2015), and in the UTLS with other model datasets (e.g., SPARC-CCMVal, 2010).

375 While the use of CMAM39-SD in this study is principally to account for sampling differences, it is useful to be aware of any biases known to affect its water vapour and ozone. Pendlebury et al. (2015) studied the representation of these two gases in CMAM30-SD between 2004 and 2010, as compared to OSIRIS v5.07 ozone and ACE-FTS v3.5 ozone and water vapour. For the former, they found that CMAM30-SD ozone is biased high compared to OSIRIS by 10–50 % in the upper troposphere of the polar and midlatitude regions, but biased low by of about 20 % in the tropics. In the lower stratosphere the difference varied, but CMAM30-SD was found to be within $\pm 10\%$ of OSIRIS ozone. Upper tropospheric biases were found to be less extreme when compared to the ACE-FTS v3.5 ozone, with differences generally peaking at 30 %, but a low bias of about 30 % was noted in October and April in the tropics. Lower stratospheric differences were found to be about 10 %, with CMAM30-SD yielding larger ozone concentrations. For water vapour, CMAM30-SD was found to be generally too dry in the UTLS, by about 10–20 % on average, with values in the tropics closer to 30 % smaller than those from ACE-FTS v3.5 (Pendlebury et al., 2015).

385 3 Methodology

To analyze the distribution of water vapour and ozone in the UTLS, equivalent latitude zonal-mean climatologies have been generated. In Sect. 3.1 the method used to generate these climatologies is outlined, which is followed by the comparison methodology in Sect. 3.2.



3.1 Climatology Generation

390 Before zonal-mean multiyear-mean UTLS climatologies can be generated from the datasets outlined in Sect. 2, the data are restricted to the same period, to permit the most direct comparisons of the trace gas climatologies. The chosen 14-year period, covering 1 June 2004 to 31 May 2018, spans from shortly after the ACE instruments began scientific operation, to shortly before the end of the CMAM39-SD model run. As many of the climatologies constructed in this study are on a 3-month (seasonal) or 12-month (full year; not shown) basis, with the former corresponding to the time required to ensure that all 395 satellite datasets can provide near-global coverage, the 14-year period analyzed was chosen to ensure an equal number of each month is present in each of these climatologies. This is done to prevent over- or under-represented months from influencing these climatologies. It should be noted that changes in the operation of each satellite instrument over time may still have an effect on the climatologies; however correcting this factor would require inherently biased data handling, paring datasets down to imitate consistent sampling, and is thus avoided.

400 In an effort to best represent atmospheric parameters by accounting for factors that may influence the distribution of trace gases, the coordinates chosen for the climatologies are tropopause-relative potential temperature and equivalent latitude. The grid for the resulting climatologies spans from 50 K below to 100 K above the tropopause over 10-K intervals in the vertical, and 5° equivalent latitude intervals are employed to span the globe in the meridional direction (e.g., 90° N–85° N, etc.). The upper and lower vertical bounds are chosen to minimize the contributions of middle stratospheric and lower tropospheric ozone 405 and water vapour to the generated climatologies.

Having established the grid for the climatologies, the grid boxes are populated with data by first interpolating the measurement and model VMR data for ozone and water vapour from their native vertical coordinates (altitude for the satellite datasets, pressure for CMAM39-SD) onto the uniform tropopause-relative potential temperature grid. To do so, the potential temperature of the lowermost 2 PVU tropopause is first subtracted from the potential temperature field for each measurement, 410 and then the resulting VMR data are interpolated onto the uniform vertical grid. Following this, the data are divided into 5° equivalent latitude bins at each vertical level. Both the tropopause and equivalent latitude information come from the JETPAC, or JETPAC-like in the case of CMAM39-SD, products generated for each dataset. Data are grouped in 1-month (not shown), 3-month, or 12-month (not shown) periods, and then for each 5° and 10-K climatology bin, the zonal-mean, median, standard deviation, median average deviation, maximum, and minimum VMR are calculated. Calculations are only performed if there 415 are a minimum of five data points available for the calculation, in order to lend a level of statistical robustness to the climatological values (e.g., Jones et al., 2012). Along with the calculated climatological fields, the total number of data points used in each bin is also provided in the derived climatologies. To evaluate the variability of the climatologies, the relative standard deviation (σ_{rel}) is used (e.g., Eckstein et al., 2017). This metric is calculated for each potential temperature/equivalent latitude climatology bin as in Eq. 1:

$$420 \quad \sigma_{rel} = \sigma / \mu, \quad (1)$$



where σ is the standard deviation and μ is the mean of the bin. This value is employed because of its independence from the magnitude of the mean concentration, which permits comparisons over the entire climatology. In addition to the multiyear-mean climatologies, climatologies have also been constructed for each individual year in the period examined.

3.2 Comparison of Climatologies

425 To evaluate the consistency of the trace gas climatologies, the relative deviation between the climatologies and a consistent reference can be used as a metric to quantify their agreement. In doing so, the relative deviation ($\delta r_{i,j}$) between a dataset and the reference is calculated for each grid point as in Eq. 2,

$$\delta r_{i,j} = 100\% \cdot \frac{[X_{i,j} - Y_{i,j}]}{X_{i,j}}, \quad (2)$$

where $X_{i,j}$ and $Y_{i,j}$ denote the VMR of the (i^{th} , j^{th}) grid cell of climatologies X and Y , with the former serving as the reference. Relative deviation is used rather than absolute deviation to account for the strong dependence of VMR on altitude
430 displayed by both trace gas distributions, by serving as a metric removed from the magnitude of the VMR gas distribution at a particular point. As the CMAM39-SD model simulation has the highest spatial density and most global coverage, climatologies derived from it have been chosen as the reference, with all other climatologies being compared to them. This choice permits the most robust comparison as it avoids the need to subsample the satellite datasets by limiting the data to only coincident pairs
435 of measurements in order to account for differences in the instruments' sampling patterns, and so the maximum number of comparisons can be made. It should be reinforced that the choice of CMAM39-SD as the reference does not purport that its trace gas simulations are more accurate than the measurements.

As previously noted in a variety of studies (e.g., Toohey and von Clarmann, 2013; Millán et al., 2016; Kolonjari et al., 2018), non-uniform sampling can lead to discrepancies in the climatological values calculated from different datasets. To
440 account for the impact of this sampling bias, comparisons have been made between the satellite climatologies and climatologies generated from model data sampled along measurement profile pathways through the atmosphere. Following the advanced sampling method of Kolonjari et al. (2018), for each satellite measurement profile, the temporally nearest three-dimensional CMAM39-SD output, which was always within 3 hours of the measurement due to the data being made available on 6 hour intervals, was identified. Without temporal interpolation, the model output was then interpolated to the potential temperature
445 levels of the matching measurement profile, using the full geolocation of the profile for the ACE instruments and the 35-km tangent measurement position for the OSIRIS profiles. The VMRs of the four nearest CMAM39-SD grid points were bilinearly interpolated to the location of the measurement profile at each vertical level to generate a model profile. The resulting sets of model VMR profiles, with one set for each gas of interest measured by each satellite instrument, were then used to generate sets of climatologies in an identical fashion to those from the satellite datasets employed in this study. The relative deviation
450 was then calculated between these subsampled CMAM39-SD datasets and the instrument datasets. Additionally, the relative difference was calculated between pairs of subsampled model climatologies, in order to explore where differences in the sampling patterns have the most pronounced impacts. For these latter comparisons, the mean of the two subsampled model climatologies was used for the term in the denominator of Eq. 2, to avoid biasing the calculated relative differences.



4 Water Vapour

455 In this section, the UTLS water vapour climatologies generated from the ACE-FTS, MAESTRO, and CMAM39-SD datasets are examined. Results shown are for the 3-month equivalent latitude zonal-mean multiyear-mean climatologies corresponding to December-January-February (DJF) and June-July-August (JJA) in order to examine and contrast the seasonal enhancement in these two gases during summer and winter.

4.1 Climatologies

460 The zonal-mean multiyear-mean climatologies from the measurement datasets (first and second columns in Fig. 1) show a roughly two order of magnitude decrease in water vapour VMR, indicating a strong vertical gradient between the upper troposphere and lower stratosphere. This gradient arises from two effects. The first is a decrease in moisture with altitude in the troposphere, resulting from the decrease in saturation vapour pressure associated with the decrease in temperatures with altitude in the troposphere. The second influence is the somewhat permeable barrier represented by the tropopause, which
465 decouples moisture-rich tropospheric air from the overlying regions outside of sporadic synoptic wave-driven mixing processes and limited vertical transport near the equator associated with the Brewer-Dobson circulation (e.g., Holton et al., 1995; Pan et al., 2004; Hoor et al., 2010). Methane oxidation provides a secondary source of water vapour in the stratosphere, but this effect is largest in the upper stratosphere and the water vapour produced by this is on the order of a few ppmv, several orders of magnitude smaller than that observed in the troposphere, hence it has no clearly identifiable influence on the distribution of
470 water vapour over much of the UTLS (e.g., Noël et al., 2018).

The meridional discontinuities in the vertical water vapour gradient, confined primarily to 10 K below to 50 K above the tropical tropopause, arise from a combination of transport effects. The regions of elevated water vapour in the midlatitudes and polar regions result from deposition of water vapour from the Brewer-Dobson circulation, while the comparatively reduced concentrations centered around the equatorial tropopause result from dehydration of air through the cold-point tropopause and
475 subsequent transport of constituents away from the tropical UTLS region. The branches of the Brewer-Dobson circulation involved here are the lowermost branches, the transition and shallow branches, which propagate up to 70 hPa and 30 hPa respectively (Holton et al., 1995; Randel et al., 2006; Lin and Fu, 2013). Because tropopause-relative coordinates are used, the result of this dehydration and transport appears as a discontinuity in the VMR gradient in both sets of seasonal climatologies for all satellite datasets. Seasonal enhancement of water vapour is evident between the two sets of seasonal climatologies, with
480 the summer hemisphere (northern for JJA, southern for DJF), showing elevated water vapour concentrations compared to the winter hemisphere as a consequence of the seasonal dehydration in winter. Lower wintertime temperatures are associated with a decrease in saturation vapour pressure, resulting in a reduced carrying capacity for water vapour in the winter hemisphere. This effect is evident in the troposphere and the lowermost 20–30 K of the stratosphere, a region where the summer hemisphere displays a consistently greater water vapour concentration than the winter hemisphere.

485 Some differences in variability are seen between the datasets (third and fourth columns in Fig. 1). The MAESTRO datasets show a larger relative standard deviation over much of the stratosphere than those from the two versions of ACE-FTS data,

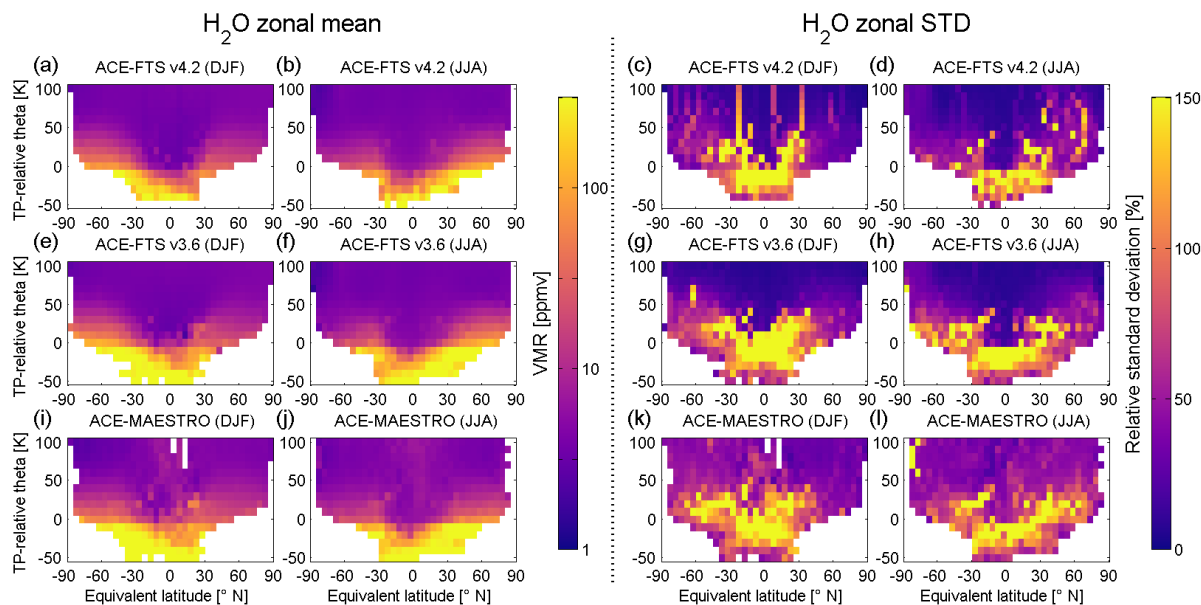


Figure 1. Three-month zonal-mean multiyear-mean (June 2004 to May 2018) water vapour climatologies constructed from the ACE-FTS v4.2 (top row), v3.6 (middle row), and MAESTRO (bottom row) datasets for DJF (first column) and JJA (second column) in tropopause-relative potential temperature and equivalent latitude coordinates. Also shown is the relative standard deviation for DJF (third column) and JJA (fourth column). Gaps in the data occur when there are either no observations made or when less than five observations are available for a given bin.

by over 50 % in regions such as the span above 50 K in the summer hemisphere. ACE-FTS v3.6 has the largest region of high variability around the tropical tropopause, with a similar meridional extent to the high-variability region in the other datasets but a greater vertical extent in these features. It also displays the greatest variability in the approximately 30 K span directly above the tropopause in the winter hemisphere in the JJA climatologies. ACE-FTS v4.2 climatologies show some prominent features that are absent in the other datasets, namely the vertical lines near 30°N/S in the DJF climatology and near 70°N in JJA. This dataset also has the most tightly confined region of elevated variability near the the tropical tropopause in both seasons. Despite these differences, broad consistency is seen in the distributions of relative standard deviation. In the area of greatest variability, centered around the tropical tropopause where there is vertical transport into the stratosphere, the consistency between measurement sets indicates that the source of this observed variability is related to underlying variations in vertical transport. Some regions of high variability extend from this region to higher latitudes in the extratropics, which is a consequence of wave-driven mixing, with asymmetry potentially stemming from hemispheric differences in the strength of this mixing. The appearance of these protrusions varies between the three datasets, indicating the potential influence of sampling biases related to the differences in the number and location of successful retrievals from each dataset. This will be explored further in the following section. Finally, the DJF climatologies show overall larger variability than that in the JJA climatologies.

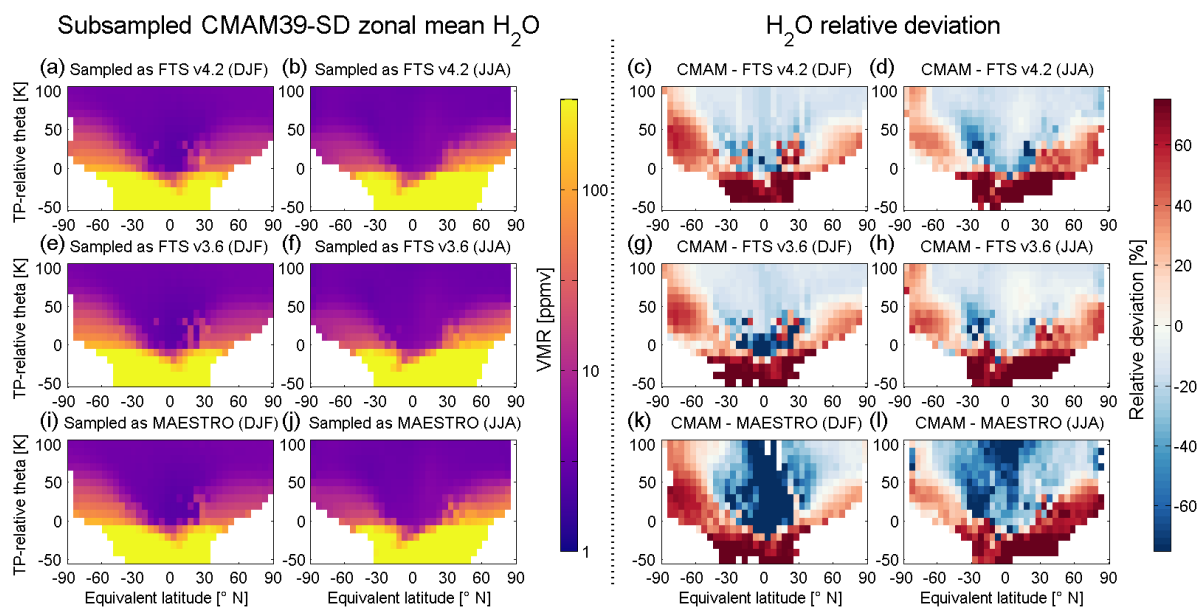


Figure 2. Comparisons between the CMAM39-SD model simulation, subsampled to the times and locations of the ACE-FTS v4.2 (top row), v3.6 (middle row), and MAESTRO (bottom row) measurements, and the satellite datasets. The zonal-mean multiyear-mean subsampled climatologies used for the comparisons are shown for DJF (first column) and JJA (second column), with the label on each plot giving the instrument measurement pattern the model is sampled with. Water vapour relative deviations (%) between measurement climatologies and the CMAM39-SD reference climatologies calculated using Eq. 2 as outlined in Sect. 3.2, are shown in the third (DJF) and fourth (JJA) columns. The colour scale of the third and fourth columns is chosen to maximize visibility; however some extreme differences can be obscured by this choice.

4.2 Comparison

While many of the prominent features are present in the climatologies constructed from each dataset, the specifics can vary, as shown in Fig. 2, which compares the climatologies constructed from CMAM39-SD, subsampled to the times and locations of the ACE-FTS v4.2 (top row), ACE-FTS v3.6 (middle row), and MAESTRO (bottom row) measurements. While the CMAM39-SD subsampled climatologies (Fig. 2 first and second columns) generally show patterns of water vapour consistent with the measurement climatologies, there are differences found in all of the subsampled climatologies (Fig. 2 third and fourth columns). Specifically, examining Figs. 1 and 2 shows significantly enhanced water vapour concentrations in CMAM39-SD over almost all of the troposphere and in the polar regions, as well as smaller water vapour concentrations near the tropical tropopause and over much of the stratosphere. The larger concentrations of CMAM39-SD water vapour in the polar regions are most prominent in the summer hemisphere, and extend further into the stratosphere in the southern hemisphere during both seasons. These differences between the model and measurement climatologies ultimately play only a minor role in this study as the main use of CMAM39-SD is to compare the measurement datasets in a consistent fashion by accounting for sampling differences.

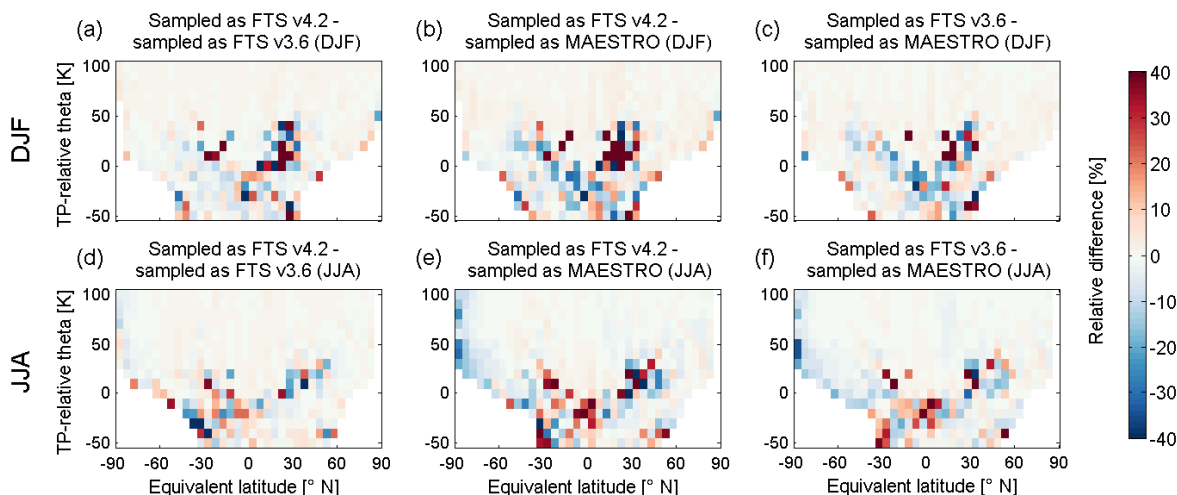


Figure 3. Intercomparisons of the CMAM39-SD model water vapour simulation, subsampled to the times and locations of the ACE-FTS v4.2, v3.6, and MAESTRO measurements, in order to assess the regions where the impact of the instruments' sampling pattern is largest. The top row corresponds to the comparisons for DJF, while the bottom row shows comparisons for JJA. Each plot title gives the two subsampled climatologies compared, with differences given as a relative difference (%). These differences are calculated as the first model subsampled climatology minus the second, and divided by the average of the two.

The CMAM39-SD subsampled model climatologies can be used to evaluate the influence of sampling on the measurement climatologies. To assess the portion of the differences between the measurement climatologies that arises from differences in sampling, whether from the measurement pattern or from the spatial and temporal distribution of successful retrievals, the sampling difference is evaluated by comparing the subsampled CMAM39-SD reference climatologies against each other, as shown in Fig. 3. Comparing these for water vapour shows that, over most of the UTLS, differences in the sampling pattern of ACE-FTS v3.6, ACE-FTS v4.2, and MAESTRO lead to only small differences in the climatologies for both periods, of approximately 4.2 % between the two ACE-FTS versions, 6.2 % between ACE-FTS v4.2 and MAESTRO, and 4.8 % between ACE-FTS v3.6 and MAESTRO, based on the average magnitude of the relative difference ($|\delta r_{i,j}|$, where the absolute value is taken to avoid oppositely signed differences cancelling each other over the entire UTLS). These differences are heavily influenced by a few areas of poor agreement in the tropical upper troposphere and lower stratosphere, outside of which the agreement is typically found to within less than 2 %. This is expected, as the two instruments make simultaneous measurements, so their sampling patterns should only differ because of differences in their retrieval processes and success rate; however, the natural variability of water vapour can emphasize small differences in this, as seen around the tropics. DJF and JJA comparisons show similar results, with the JJA comparisons having slightly better agreement, by about 0.2–1.0 %. The upper troposphere shows larger absolute differences than those in the lower stratosphere, by about 3–5 % as averaged over the two regions. This comparison is influenced by the small differences previously noted near 50 K above the tropopause, which decreases the lower stratospheric average difference. Where large differences are observed, the greatest differences occur in the region spanning



530 0–20 K above the tropopause and approximately 15–30°N. Over this small span, differences are mostly on the order of about 70 %, with one to two grid cells per comparison yielding differences in excess of 100 %, with these latter differences likely resulting from outlier measurements. Note that differences in excess of 40 % are not visible as the colour scale was chosen to emphasize differences over the entire UTLS at the cost of these large differences blending together. However, outside these few grid cells the subsampled model climatologies show overall excellent agreement, with differences of less than 5 %, indicating
535 only a small sampling difference between the three water vapour datasets, as expected from their shared measurement pattern. Furthermore, the regions of greatest differences are coincident with the regions of highest variability, as shown in Fig. 1, a consequence of the range of VMR values observed in these regions and the impact of sampling on their averages.

Having quantified the influence of the instruments' sampling patterns, focus can turn to comparing the measurement climatologies using the subsampled CMAM39-SD climatologies, in Fig. 2, as a reference. Over nearly the entirety of the upper
540 troposphere during the DJF (JJA) period, the subsampled CMAM39-SD climatologies yield elevated levels of water vapour, with average differences of approximately 69 % (73 %) compared to ACE-FTS v4.2, 65 % (69 %) compared to ACE-FTS v3.6, and 65 % (66 %) compared to MAESTRO. Overall, the three measurement climatologies agree to within 4 % in DJF, and 7 % in JJA, with better agreement found between ACE-FTS v3.6 and both other datasets than between ACE-FTS v4.2 and MAESTRO. The remainder of the regions in which CMAM39-SD displays greater water vapour VMRs than the measure-
545 ment datasets can be subdivided into the spans north and south of approximately 45° from 0–70 K above the tropopause. The southern of these regions yields, in DJF (JJA), differences that are 42 % (23 %), 36 % (28 %), and 51 % (20 %) larger in the model than ACE-FTS v4.2, ACE-FTS v3.6, and MAESTRO. North of 45°, these differences in DJF (JJA) are 22 % (34 %), 24 % (33 %), and 21 % (50 %). Over these two regions and periods, the agreement is variable, with some comparisons showing agreement to within 5 % in DJF and as large as 17 % in JJA (e.g., in the northern lower stratosphere). Altogether, these findings
550 indicate that the satellite datasets are in generally good agreement across these regions. Note that there is a seasonal influence on the differences, with the measurements showing better agreement with CMAM39-SD and each other during the winter season in each hemisphere.

In the tropical lower stratosphere, the model-derived climatologies, shown in Fig. 2, display smaller water vapour concentrations than those derived from the measurement datasets; this region also corresponds to where the poorest agreement is found
555 between the satellite datasets. The average DJF (JJA) model-measurement deviation for the three measurement datasets is 17 % (19 %) and 25 % (15 %) for ACE-FTS v4.2 and v3.6; however the comparison with MAESTRO yields much greater differences of 83 % (41 %). The cause of this increased water vapour concentration in the MAESTRO dataset is tied to the upper altitude bound of the MAESTRO retrieval, which is lower when the lower stratosphere is drier, and vice-versa, leading to observations of wetter conditions primarily populating higher altitude locations, such as the tropical lower stratosphere. For ACE-FTS, the
560 model-measurement comparison differences in the stratosphere during JJA are greatest over a region approximately 25° wide spanning 40 K in the vertical centered near 30° S and 40–50 K above the tropopause. In DJF, the greatest difference between ACE-FTS v3.6 and the model occurs over an approximately 45° and 30 K region centered around the tropical tropopause, while for ACE-FTS v4.2 only a few grid cells in this region show large differences. Because of the greater consistency in JJA than in DJF, the two versions of ACE-FTS are in better agreement in the former period than in the latter, with the former agreeing



565 to within 5 %, while the latter shows differences of 8 %. In contrast, the large model-measurement differences displayed in the MAESTRO comparisons are not nearly as spatially limited, and align poorly with the two versions of ACE-FTS studied. This apparent overabundance of MAESTRO water vapour in the tropical lower stratosphere, as compared to both CMAM39-SD and ACE-FTS, varies between the two seasons shown, with more extreme differences observed over a larger portion of the lower stratosphere in DJF than in JJA. Thus poor agreement, with differences of 22–66 %, is found between the two versions
570 of ACE-FTS and MAESTRO over this region in both seasons, but within this large range of differences, the agreement in the JJA climatologies is significantly better than that in the DJF climatologies by about 40 %.

Overall there is a clear discrepancy between the model and satellite datasets, with the former yielding elevated water vapour concentrations over the troposphere and polar stratosphere, while showing drier conditions over much of the remaining stratosphere. Despite this, the CMAM39-SD subsampled model climatologies are valuable for assessing the impact of sampling.
575 The measurement datasets show mixed relative performance, with the two ACE-FTS versions showing very good agreement throughout most of the UTLS, with differences of less than 10 %, while the MAESTRO climatologies show varied agreement with the two ACE-FTS versions, with differences ranging from less than 5 % to over 80 %, varying based on location and season. In considering the entire UTLS, from 50 K below to 100 K above the tropopause, the ACE-FTS v4.2 climatologies have an average absolute difference from CMAM39-SD of 28 % (29 %) in DJF (JJA), while ACE-FTS v3.6 comparisons yield a 35 %
580 (28 %) difference, and MAESTRO comparisons a 69 % (44 %) difference. Part of the large difference seen in the MAESTRO comparisons result from the upper bound of the MAESTRO water vapour measurements near 22 km, where measurements tend to possess a high degree of uncertainty due to the worsening quality of MAESTRO water vapour retrievals with altitude. The altitudes included in these tropopause-relative climatologies are higher in the tropics than at the poles because the tropical tropopause is at higher altitude, so the lower-quality MAESTRO measurements from near its upper bound would have
585 a larger influence in the tropics than at the poles in the lower stratosphere. The wet bias in MAESTRO water vapour found here agrees with estimates by Lossow et al. (2019) and Hegglin et al. (2021). While there is overall poor agreement between MAESTRO and ACE-FTS climatologies in DJF, with differences of approximately 40 %, in JJA the overall difference is about 16 %, which is in much better agreement. Some regions of the UTLS show even better agreement, namely the upper troposphere and extratropical lower stratosphere, where the influence of the upper limit to the MAESTRO water vapour product is
590 less impactful. Thus the MAESTRO dataset still provides valuable insight into water vapour in the UTLS, a finding supported by prior validation efforts (e.g., Lossow et al., 2019).

5 Ozone

In this section, the UTLS ozone climatologies generated from the ACE-FTS, MAESTRO, OSIRIS, and CMAM39-SD datasets are examined. As with water vapour above, results shown are based on seasonal (3-month) climatologies for DJF and JJA.

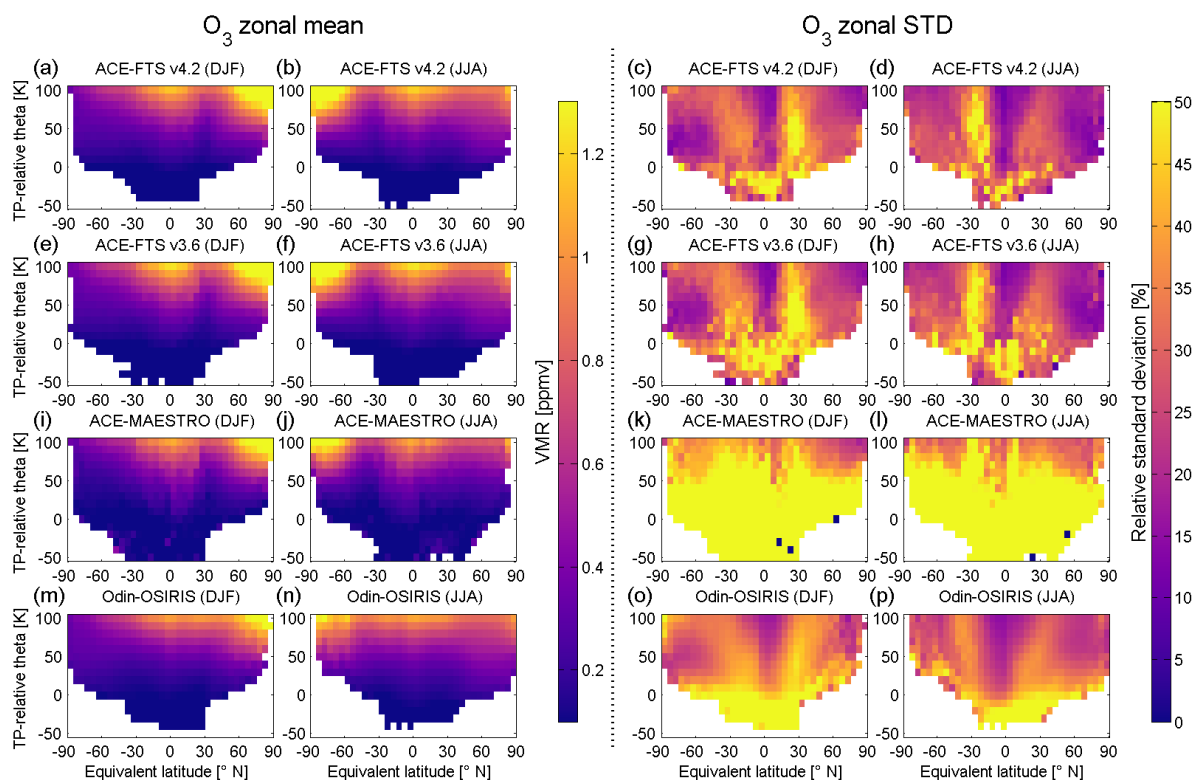


Figure 4. Same as Fig. 1, but for ozone, and including an additional row (fourth row) for climatologies constructed from the OSIRIS dataset. The MAESTRO relative standard deviation is shown on a logarithmic colour scale in Fig. 7 to better illustrate the large values observed.

595 5.1 Climatologies

Many features of the equivalent latitude zonal-mean multiyear-mean ozone climatologies (first and second columns in Fig. 4) are consistent among the datasets, with the most prominent feature being the clear gradient in ozone extending from a nearly uniform minimum below 30–50 K above the tropopause to VMR values nearly an order of magnitude greater near the top of the UTLS. All the ozone datasets show relatively uniformly small values, approximately 0.05–0.1 ppmv, below the tropopause. This feature arises because the tropopause acts as a transport barrier, largely confining higher ozone values to the stratosphere, while the reactivity of ozone as an oxidizing agent prevents it from becoming well-mixed over time (Lelieveld and Dentener, 2000; Brasseur and Solomon, 2005). The observed vertical gradient in UTLS ozone is steepest in the tropics and the winter polar region, the two regions where the concentration of UTLS ozone is largest at the upper limit of the climatologies. These two local maxima arise from different processes, discussed in further detail below, with the underlying difference leading to the seasonal dependence of the polar ozone maximum location, as compared to the fairly static tropical feature.

The tropical ozone peak is associated with the relative proximity of the tropical tropopause to the ozone concentration maximum in the middle stratosphere. Outside of the winter pole, the altitude of the ozone maximum in the mid-stratosphere

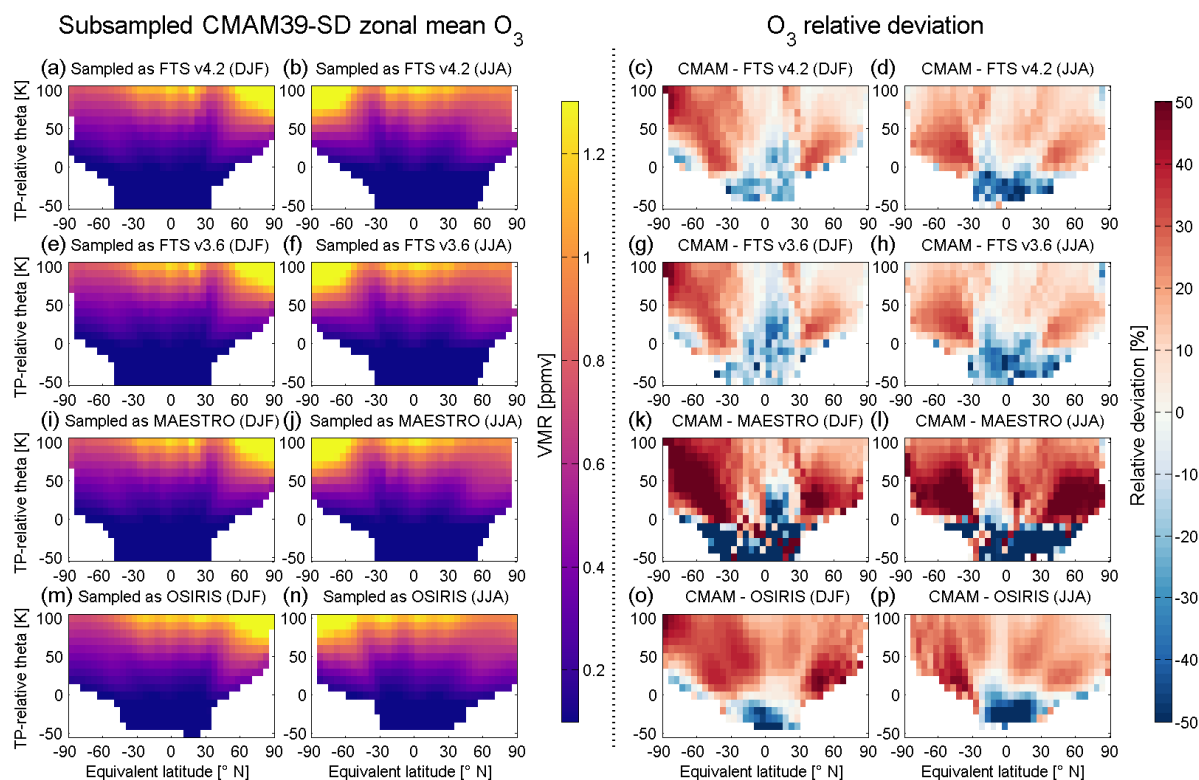


Figure 5. Same as Fig. 2, but for ozone and including an additional row (fourth row) for climatologies constructed from the CMAM39-SD simulation subsampled to the location and time of the OSIRIS measurements and for the comparisons between these and the OSIRIS ozone climatologies.

somewhat mimics the shape of the tropopause, appearing lower in altitude near the poles as compared to the tropics; however this curvature is less pronounced than that of the tropopause. As such, outside of the winter pole, there is a greater difference
 610 in altitude between the ozone maximum and the tropopause at the poles than in the tropics. The result of this is the inclusion of air from nearer to the stratospheric ozone maximum within the upper bounds of the UTLS in the tropics, but not to the same extent outside of this region. This directly leads to the larger concentration of ozone observed in Fig. 4 at higher altitudes in the tropics. The other key feature of these climatologies is the season-dependent stratospheric maximum over the winter pole, which extends further into the lower stratosphere than the tropical peak. Ozone is transported throughout the stratosphere via
 615 circulation processes, including those associated with the Brewer-Dobson circulation, with seasonal variations of these patterns leading to the observed enhanced ozone feature over the winter pole. Specifically, within the winter stratospheric polar vortex, the diabatic descent of cold air masses as part of the meridional overturning circulation carries ozone downwards from higher in the stratosphere, enhancing the ozone concentration in the lower stratosphere during the winter months.

The aforementioned ozone features are present in all of the satellite climatology datasets, but there is variation between
 620 their appearance in each. Polar ozone is similarly distributed for the two ACE-FTS climatologies, but the MAESTRO distri-

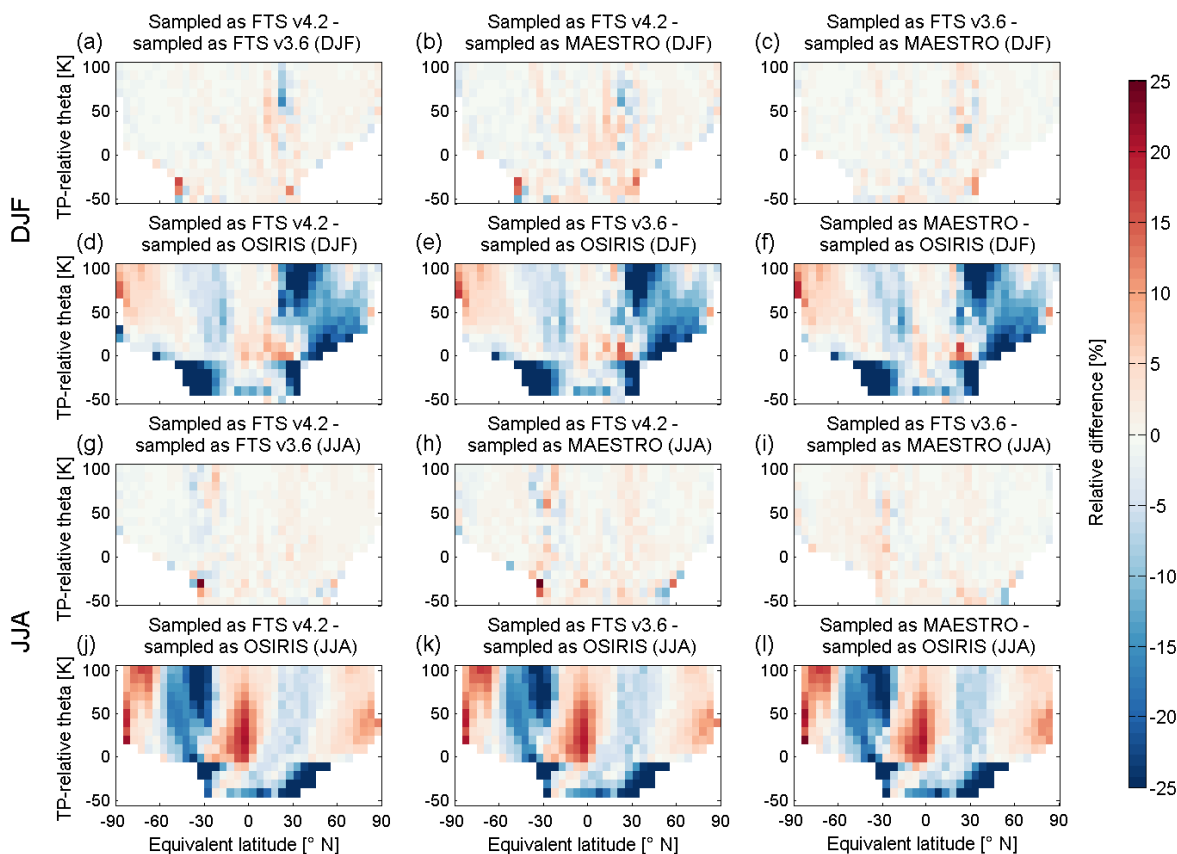


Figure 6. Same as Fig. 3, but for ozone, and including an additional two rows for comparisons involving climatologies constructed from the OSIRIS measurement pattern. Note that the DJF and JJA comparisons are now spread over two rows each, with the top two rows corresponding to the former, and the bottom two to the latter.

butions display a somewhat reduced feature and OSIRIS a still smaller feature. These features in the MAESTRO and OSIRIS climatologies are found to cover both a narrower meridional swath and extend less deeply into the UTLS. As shown in the sub-sampled CMAM39-SD climatologies in Fig. 5 (first and second columns), there is little variation in ACE-FTS and MAESTRO sampling of this feature, indicating that this difference is most likely related to the ozone products themselves. This is supported
 625 by the comparison of the CMAM39-SD subsampled climatologies in Fig. 6, which emphasizes that there is little difference between the ACE-FTS and MAESTRO sampling patterns for ozone. Part of the product difference might be attributable to the higher vertical resolution of the MAESTRO instrument compared to that of ACE-FTS, but this cannot be disentangled from other potential sources for this discrepancy. The OSIRIS sampling pattern, in contrast, does lead to changes in the appearance of the polar ozone distribution, likely accounting for at least a portion of the reduced size observed for this feature. The tropical maximum also varies between the climatologies, appearing largest for ACE-FTS v3.6, and progressively smaller for ACE-FTS
 630

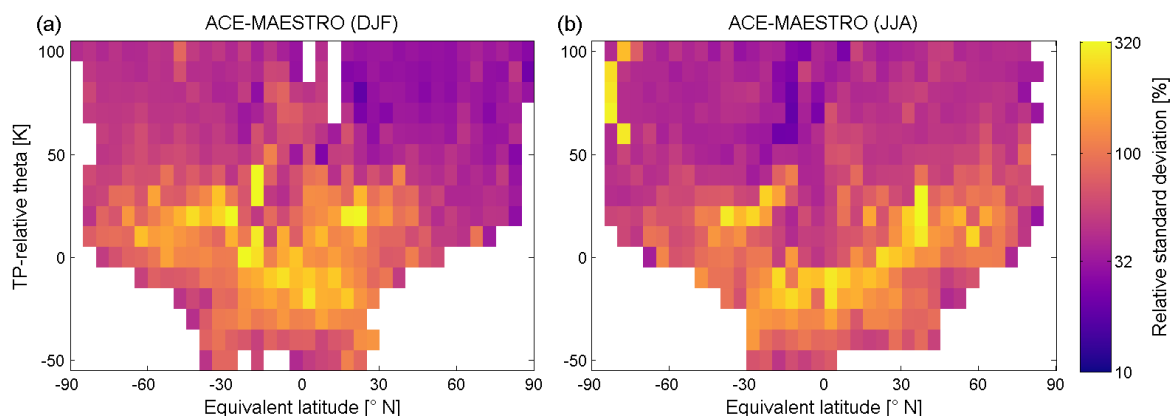


Figure 7. Alternative view of the MAESTRO ozone relative standard deviation, as first presented in panels (k) and (i) from Fig. 4, with (a) here corresponding to (k), and likewise (b) to (i). Note the shift to a logarithmic colour scale to better display the variability.

v4.2 and MAESTRO. The OSIRIS feature covers a smaller vertical range than that in the two ACE-FTS versions, and a similar range to that from MAESTRO, but extends further poleward than the other datasets and merges with the maximum over the polar region. While the depth of the tropical feature appears fairly consistent between the four sets of subsampled CMAM39-SD climatologies in Fig. 5, the extension of the high ozone feature across the midlatitudes and into the polar region is seen only in
635 the one set of CMAM39-SD subsampled climatologies, those subsampled to the OSIRIS measurement pattern, indicating that the feature is associated with sampling differences, which is supported by the comparisons shown in Fig. 6.

As with the distribution of mean ozone, the variability displayed by each set of climatologies (columns three and four in Fig. 4) is characterized by a series of broadly consistent features, but with quantitative differences between the datasets. The general patterns of variability include two lower stratospheric regions of high variability, one in each hemisphere around 35°,
640 that extend from the tropopause to the top of the UTLS climatologies and show more variability in the winter than in the summer hemisphere. These regions roughly border the edge between the upwelling and downwelling portions of the Brewer-Dobson circulation, so variable wave activity is a likely source of this variability as air parcels are sporadically mixed along isopleths (Plumb, 2002; Lin and Fu, 2013; Butchart, 2014). The appearance of the regions of highest variability is generally consistent between the two versions of ACE-FTS, but in the OSIRIS climatologies these regions are distributed over a larger meridional
645 swath. In addition, the maximum values in these regions are smaller for the OSIRIS climatologies than for those derived from the two versions of ACE-FTS. Differences in the sampling patterns of each instrument are a likely cause of this difference between the datasets. High relative standard deviation values are also found in the troposphere for the ACE-FTS and OSIRIS climatologies, which may be influenced by there being fewer successful measurements by either instrument in this low-altitude region. This tropospheric variability extends to cover the entire troposphere in the OSIRIS climatologies, while remaining
650 concentrated near the tropics for ACE-FTS. The MAESTRO climatologies presented in Fig. 4 do not clearly display any of these relative standard deviation features, instead their variability distributions appear to be almost uniformly large throughout



most of the UTLS when plotted using the same colour scale as for ACE-FTS and OSIRIS. Examining the distribution of MAESTRO variability in further detail on a logarithmic scale, as done in Fig. 7, reveals that it appears as a general gradient that decreases with altitude without much of the structure observed for other instruments, with the exception of the highest variability occurring near the tropical tropopause. As noted in Sect. 2.2, despite the filtering applied to the MAESTRO ozone dataset removing 8.9 % of the available profiles, the variability in the retrievals is too great to reliably identify all outliers. While this does not inhibit the use of MAESTRO in evaluating the consistency of these Canadian limb sounders, this does indicate that this v3.13 MAESTRO ozone product should be used with caution, in spite of the apparent agreement between most features of the ozone distributions derived from it and those from the other datasets employed in this study.

660 5.2 Comparison

The CMAM39-SD model dataset is used to evaluate the consistency between these measurement datasets as done for water vapour. Figure 5 shows DJF and JJA ozone climatologies generated from CMAM39-SD sampled to the times and locations of the ACE-FTS v4.2 (top row), v3.6 (second row), MAESTRO (third row), and OSIRIS (bottom row) measurements, as well as the comparison between these and the associated satellite climatologies. The subsampled model climatologies display very similar patterns in their ozone distributions to those in the measurement climatologies in Fig. 4, with the largest differences occurring in the summer hemisphere over the polar region where the model yields greater ozone VMRs above 60–70 K above the tropopause. The set of model-measurement comparisons (Fig. 5 third and fourth columns) further reveals that CMAM39-SD yields larger ozone concentrations than the measurement datasets outside the tropical lower stratosphere and smaller ozone concentrations than those datasets over the upper troposphere and in some instances in the tropical lower stratosphere. As with the water vapour comparisons, these differences between the model simulation and the measurements does not limit the use of the model to evaluate the consistency of the measurement datasets.

The subsampled CMAM39-SD climatologies in Fig. 6 aid in evaluating sampling effects. In evaluating the differences between the CMAM39-SD subsampled ozone climatologies, the average magnitude of the difference between the model climatologies generated using the times and locations of the ACE-FTS v4.2, ACE-FTS v3.6, and MAESTRO measurements is 1–2 %. The closest agreement for these three datasets, of 1.2 %, was found between the climatologies generated from the ACE-FTS v3.6 and MAESTRO measurement patterns, while the worst agreement, 1.7 %, was noted between the climatologies for ACE-FTS v4.2 and MAESTRO. Agreement is similar in the two seasons shown, with less than a 0.3 % change in the average comparisons between seasons. Thus their measurement patterns lead to negligible differences between the three datasets, with excellent agreement to better than 2 %, as expected for two instruments that share a line-of-sight for measurements of a gas that does not vary as extremely as water vapour. Greater differences are noted when comparing the subsampled model climatologies made using the OSIRIS measurement pattern to the others. The set of subsampled climatologies generated from the OSIRIS measurement pattern is found to differ by 9 % on average from the other three instrument-subsampled climatologies, but differences as large as 76 % are observed in a subset of the grid cells, mostly confined to the upper troposphere. The OSIRIS measurement pattern leads to alternating regions of larger and smaller concentrations but the majority of these differences are constrained to the $\pm 25\%$ range with better agreement found between the measurement patterns in the summer hemisphere.



This generally fits with the finding of Sheese et al. (2021), where the 2σ geophysical variability of O_3 between coincident ACE-FTS and OSIRIS measurements was estimated to be on the order of about 5–50 % in the lower stratosphere, depending on latitude and coincidence criteria. Based on these comparisons, the OSIRIS measurement pattern leads to generally smaller concentrations of ozone in the upper troposphere. Overall, the OSIRIS measurement pattern leads to model subsampled climatologies that generally agree with the other three subsampled climatologies. In contrast to the results for water vapour, the ozone variability observed in Fig. 4 does not correspond to the regions of disagreement between the subsampled climatologies, indicating that the difference is mostly due to the sampling pattern rather than variability in ozone itself. Thus, this disagreement arises from differences between the two ACE instruments and OSIRIS in their latitudinal coverage and the timing of their observations throughout the two seasons analyzed.

Differences in instrument climatologies from the CMAM39-SD subsampled climatologies (Fig. 5) show that the subsampled model yields smaller ozone concentrations than the measurements in the upper troposphere, and larger concentrations outside of the tropics in the lower stratosphere. Below the tropopause, the model-measurement differences are largest for comparisons with MAESTRO, and smallest for comparisons with the two sets of ACE-FTS climatologies. Quantitatively, the relative difference below the tropopause between the DJF (JJA) subsampled CMAM39-SD ozone distributions and those from the instruments is approximately 15 % (26 %) for ACE-FTS v4.2, 12 % (23 %) for ACE-FTS v3.6, 106 % (91 %) for MAESTRO, and 19 % (37 %) for OSIRIS. The two versions of ACE-FTS are found to agree closely, to within 3 %, over the upper troposphere, while ACE-FTS v4.2 agrees to within 11 % of OSIRIS, and ACE-FTS v3.6 to within 14 % of OSIRIS. In JJA the agreement between ACE-FTS and OSIRIS worsens somewhat, such that the differences are approximately twice as large as those in DJF. In contrast to this general agreement, the MAESTRO ozone climatology agrees poorly with the others below the tropopause, with the smallest difference being 54 %.

In the lower stratosphere, the subsampled model climatologies show generally larger ozone concentrations than the four measurement datasets, with some exceptions in part of the tropics during DJF. Specifically, the subsampled model climatologies show smaller ozone VMRs than the ACE-FTS v4.2 and MAESTRO climatologies in DJF in the tropics between the tropopause and approximately 50 K above the tropopause. In comparison to the ACE-FTS v3.6 DJF climatology, the subsampled model yields smaller VMRs up to about 100 K above the tropopause; however this difference is largest between the tropopause and about 50 K above the tropopause. For these three datasets, the differences occur primarily between about 5°S and 25°N, and successively greater ozone concentrations are seen in the ACE-FTS v4.2, ACE-FTS v3.6, and MAESTRO climatologies. The average model-measurement differences over this region in DJF are 12 %, 21 %, and 32 % for ACE-FTS v4.2, ACE-FTS v3.6, and MAESTRO respectively, translating to ACE-FTS v3.6 agreeing with the other two datasets to within 11 %, while the MAESTRO and ACE-FTS v4.2 climatologies show a 20 % general difference. The model comparison with the OSIRIS DJF climatology over this region of the tropical lower stratosphere leads to a model-measurement difference of 13 %. These model-measurement differences are in poor agreement with those of the other instruments as the model is found to possess smaller ozone VMRs than OSIRIS over this span, with the closest agreement, of 25 %, found between OSIRIS and ACE-FTS v4.2. In JJA the model yields generally greater ozone VMRs than the three ACE datasets, outside of a few grid cells, as it does in both seasons as compared to OSIRIS.



Outside the tropical lower stratosphere in DJF, the subsampled model climatologies generally display more ozone than the four measurement datasets in the lower stratosphere, with exception for the region 0–20 K above the tropopause south of 60°S, where the model exhibits less ozone than the measurements. For the regions where there is greater model ozone, model-measurement differences are larger in the southern hemisphere than in the northern, with the MAESTRO comparisons showing the largest difference from the model while the two ACE-FTS versions show the smallest differences, in agreement with Hegglin et al. (2021). When averaged over the lower stratosphere, with exception of the span between 5°S and 25°N noted above, the model-measurement differences are 17 % (15 %) for ACE-FTS v4.2, 18 % (14 %) for ACE-FTS v3.6, 31 % (33 %) for MAESTRO, and 26 % (19 %) for OSIRIS in DJF (JJA). Model-measurement differences in the lower stratosphere of the southern hemisphere are 22 % (17 %) for ACE-FTS v4.2, 22 % (17 %) for ACE-FTS v3.6, 36 % (33 %) for MAESTRO, and 29 % (23 %) for OSIRIS in DJF (JJA). In the lower stratosphere of the northern hemisphere, model-measurement differences are 11 % (13 %) for ACE-FTS v4.2, 12 % (11 %) for ACE-FTS v3.6, 24 % (34 %) for MAESTRO, and 24 % (16 %) for OSIRIS in DJF (JJA). These model-measurement comparisons imply agreement to within 2 % for the two ACE-FTS versions. The MAESTRO comparisons with the two versions of ACE-FTS yield differences of 13–23 %, with better agreement in DJF than in JJA by 2–10 %. OSIRIS typically agrees better with MAESTRO in DJF and with ACE-FTS in JJA; the DJF differences between MAESTRO and OSIRIS are less than 5 % and those between OSIRIS and ACE-FTS are 8–13 %, while in JJA these differences are 10–18 % and 3–6 % respectively.

In summary, the ozone climatologies from the satellite datasets show similar features, but there are moderate differences in their comparisons to CMAM39-SD, and by extension each other. In the upper troposphere, the subsampled CMAM39-SD climatologies used for comparisons yield smaller ozone VMRs than those for the instrument climatologies, with the two versions of ACE-FTS displaying the least ozone, followed by the OSIRIS and then the MAESTRO climatologies, which yield the greatest VMRs. This is reversed over much of the stratosphere, except for a portion of the tropics where the model shows less ozone than three of the measurement datasets in DJF. With few exceptions there is agreement to within 10 % between the OSIRIS and ACE-FTS climatologies, with average model-measurement differences over the UTLS in DJF (JJA) of 16 % (16 %) for ACE-FTS v4.2, 16 % (15 %) for ACE-FTS v3.6, and 25 % (21 %) for OSIRIS. The MAESTRO ozone climatologies were found to agree fairly poorly with those from ACE-FTS, and only somewhat better with OSIRIS, with average model-measurement differences of 49 % (47 %) in DJF (JJA) over the entire UTLS. The disagreement of the MAESTRO ozone climatologies with those of the other datasets, coupled to the high degree of variability observed for this product, supports the conclusion that the v3.13 MAESTRO dataset should be used with caution, as it shows the least consistency with other instruments. In contrast, the results for the other three datasets demonstrate their value for UTLS ozone studies

6 Summary

To meet the need for UTLS-focused climatologies, generated with the goal of minimizing the effects of geophysical variability, and in support of the OCTAV-UTLS project, new climatologies have been constructed for water vapour and ozone from 14 years of data measured by three Canadian limb-sounding instruments: ACE-FTS (v3.6 and v4.2 water vapour and ozone),



755 MAESTRO (v31 water vapour, v3.13 ozone), and OSIRIS (v5.10 ozone only). These climatologies employ tropopause-relative potential temperature and equivalent latitude coordinates in an effort to best represent the distribution of these two gases in the UTLS by accounting for sources of variability (Pan et al., 2004; Hoor et al., 2004; Hegglin et al., 2008). The distribution of these two gases, and their variability, have been examined for two seasons, DJF and JJA. To evaluate their consistency in representing UTLS water vapour and ozone, these measurement climatologies have been compared to reference climatologies generated from the CMAM39-SD model, subsampled to the times and locations of the measurements made by each instrument. 760 These subsampled model climatologies provide a consistent reference to assess the agreement of the instrumental datasets, as well as to explore the influence of different measurement patterns on the datasets.

In comparing the water vapour climatologies, better than 8 % overall differences were found between the two versions of ACE-FTS. Agreement with MAESTRO was more varied, with comparisons against the two versions of ACE-FTS showing agreement ranging from less than 5 % to over 60 %, with the DJF climatologies showing typically poorer agreement than those 765 for JJA. These comparisons are influenced by the upper bound of the MAESTRO water vapour product around 17–22 km, and the large uncertainty associated with its measurements near this boundary. It should be noted that ACE-FTS v3.6 showed better agreement with MAESTRO than ACE-FTS v4.2 did; but this is influenced by the MAESTRO product using the v3.6 temperature and pressure information in its retrievals, which has been shown to lead to a drift in the ACE-FTS v3.6 data (Sheese et al., 2022).

770 Comparisons of the ozone climatologies yielded typically better agreement between the four measurement datasets than seen for water vapour. The two versions of ACE-FTS agree closely with differences typically less than 2 %, while results for OSIRIS agreed with those from the two ACE-FTS climatologies with an overall less than 10 % difference. As with water vapour, MAESTRO ozone was found to differ from the other datasets more significantly. MAESTRO showed the best agreement with OSIRIS, but overall differences were on the order of 25 %, while comparisons to ACE-FTS yielded agreement that was 775 somewhat worse, by about 5–10 %, than with OSIRIS. Part of this disagreement stems from the MAESTRO ozone product displaying significantly higher variability than the other ozone datasets, preventing statistical filtering from reliably removing all outlier measurements using the method of Sheese et al. (2015), but overall the large disagreement suggests that the v3.13 MAESTRO ozone product should be used with caution.

In addition to assessing the agreement of the measurement climatologies, the subsampled model climatologies allowed 780 for evaluation of the influence of sampling patterns on the representation of water vapour and ozone in the UTLS. These subsampled model climatologies can be directly compared in order to determine where differences in sampling, whether from the measurement patterns or from the spatial and temporal distribution of successful retrievals, lead to differences in the climatologies. It was found that the high variability of upper tropospheric water vapour can lead to large differences even when comparing subsampled model climatologies generated from nearly identical sampling patterns, such as those for 785 the two versions of ACE-FTS. Thus, even relatively small differences in sampling patterns can have a large effect on water vapour measurement climatologies in the UTLS. Contrasting this, the close agreement observed for the subsampled ozone model climatologies produced with similar sampling patterns indicates that mean ozone VMRs are less sensitive to underlying variability in ozone. However, differences in sampling patterns can still have a noticeable effect, such as the difference observed



790 between the OSIRIS subsampled climatologies and those from ACE-FTS and MAESTRO. Overall, the choice of instruments employed in this study allows for the evaluation of key factors, namely atmospheric variability and sampling differences, that can influence differences in UTLS-focused climatologies of these species.

795 *Data availability.* ACE-FTS v3.6 and v4.2 data, as well as MAESTRO v3.13 ozone and v31 water vapour, are available from <https://databace.scisat.ca/level2/>. Access to these products requires registration. Data quality flags for ACE-FTS v4.1/4.2 are available from <https://doi.org/10.5683/SP2/BC4ATC>. OSIRIS v5.10 ozone data are available at <ftp://odin-osiris.usask.ca/>. CMAM39-SD data were downloaded from ftp://crd-data-donnees-rdc.ec.gc.ca/pub/CCCMA/dplummer/CMAM39-SD_6hr. JETPAC products for these instruments are available at <https://mls.jpl.nasa.gov/eos-aura-mls/dmp>. Access to these products requires registration. For the climatologies constructed for this work please contact the authors.

800 *Author contributions.* This study was designed by PSJ and KAW with input from GLM and LM. PSJ wrote the manuscript and performed the analyses, building on prior work from NJR. CDB and PES provided their expertise on ACE-FTS; CES, JZ, and CTM on ACE-MAESTRO; DD and CES on the Odin-OSIRIS; and DAP on CMAM39-SD. GLM and LM provided the JETPAC meteorological product files for the satellite instruments, and code used to generate JETPAC-like products from the CMAM39-SD dataset. PES created the data flags for the ACE-FTS and ACE-MAESTRO data products. Valuable comments on the manuscript were provided by all authors.

Competing interests. The authors declare that they have no conflict of interest.

805 *Acknowledgements.* This project is supported by a grant from the Canadian Space Agency (CSA). The Atmospheric Chemistry Experiment (ACE), also known as SCISAT, is a Canadian-led mission mainly supported by CSA. We thank Peter Bernath for his leadership of the ACE mission. The development of the CMAM39-SD dataset was funded by the CSA. We thank Ted Shepherd, Dylan Jones, John Scinocca, and David Plummer for their leadership and support of the CMAM39-SD Project. Odin is a Swedish-led satellite project funded jointly by Sweden (Swedish National Space Board), Canada (CSA), France (Centre National d'Etudes Spatiales), and Finland (Tekes), with support by the Third-Party Mission program of the European Space Agency (ESA). This study was partially-funded by ESA (Contract No. 4000123554) 810 via the Water_Vapour_cci project of ESA's Climate Change Initiative (CCI). Work at the Jet Propulsion Laboratory, California Institute of Technology, was done under contract with the US National Aeronautics and Space Administration. GLM was supported by subcontract number 1521127 from the Jet Propulsion Laboratory.



References

- Adams, C., Bourassa, A. E., Bathgate, A. F., McLinden, C. A., Lloyd, N. D., Roth, C. Z., Llewellyn, E. J., Zawodny, J. M., Flittner, D. E.,
815 Manney, G. L., Daffer, W. H., and Degenstein, D. A.: Characterization of Odin-OSIRIS ozone profiles with the SAGE II dataset, *Atmos. Meas. Tech.*, 6, 1447–1459, <https://doi.org/10.5194/amtd-6-1033-2013>, 2013.
- Adams, C., Bourassa, A. E., Sofieva, V., Froidevaux, L., McLinden, C. A., Hubert, D., Lambert, J.-C., Sioris, C. E., and Degenstein, D. A.:
Assessment of Odin-OSIRIS ozone measurements from 2001 to the present using MLS, GOMOS, and ozonesondes, *Atmos. Meas. Tech.*,
7, 49–64, <https://doi.org/10.5194/amt-7-49-2014>, 2014.
- 820 Bernath, P. F.: The Atmospheric Chemistry Experiment (ACE), *J. Quant. Spectrosc. Ra.*, 186, 3–16,
<https://doi.org/10.1016/j.jqsrt.2016.04.006>, 2017.
- Bernath, P. F., McElroy, C. T., Abrams, M. C., Boone, C. D., Butler, M., Camy-Peyret, C., Carleer, M., Clerbaux, C., Coheur, P.-F., Colin, R.,
DeCola, P., DeMazière, M., Drummond, J. R., Dufour, D., Evans, W. F. J., Fast, H., Fussen, D., Gilbert, K., Jennings, D. E., Llewellyn,
E. J., Lowe, R. P., Mahieu, E., McConnell, J. C., McHugh, M., McLeod, S. D., Michaud, R., Midwinter, C., Nassar, R., Nichitiu, F.,
825 Nowlan, C., Rinsland, C. P., Rochon, Y. J., Rowlands, N., Semeniuk, K., Simon, P., Skelton, R., Sloan, J. J., Soucy, M.-A., Strong,
K., Tremblay, P., Turnbull, D., Walker, K. A., Walkty, I., Wardle, D. A., Wehrle, V., Zander, R., and Zou, J.: Atmospheric Chemistry
Experiment (ACE): Mission overview, *Geophys. Res. Lett.*, 32, L15S01, <https://doi.org/10.1029/2005GL022386>, 2005.
- Bognar, K., Zhao, X., Strong, K., Boone, C. D., Bourassa, A. E., Degenstein, D. A., Drummond, J. R., Duff, A., Goutail, F., Griffin, D.,
Jeffery, P. S., Lutsch, E., Manney, G. L., McElroy, C. T., McLinden, C. A., Millán, L. F., Pazmino, A., Sioris, C. E., Walker, K. A., and
830 Zou, J.: Updated validation of ACE and OSIRIS ozone and NO₂ measurements in the Arctic using ground-based instruments at Eureka,
Canada, *J. Quant. Spectrosc. Ra.*, 238, 106 571, <https://doi.org/10.1016/j.jqsrt.2019.07.014>, 2019.
- Boone, C. D., Nassar, R., Walker, K. A., Rochon, Y., McLeod, S. D., Rinsland, C. P., and Bernath, P. F.: Retrievals for the atmospheric
chemistry experiment Fourier-transform spectrometer, *Appl. Optics.*, 44, 7218–7231, <https://doi.org/10.1364/AO.44.007218>, 2005.
- Boone, C. D., Walker, K. A., and Bernath, P. F.: Version 3 retrievals for the Atmospheric Chemistry Experiment Fourier Transform Spec-
835 trometer (ACE-FTS), in: *The Atmospheric Chemistry Experiment ACE at 10: A Solar Occultation Anthology*, pp. 103–127, A. Deepak
Publishing, Hampton, Virginia, U.S.A., 2013.
- Boone, C. D., Bernath, P. F., Cok, D., Jones, S. C., and Steffen, J.: Version 4 retrievals for the atmospheric chemistry experiment Fourier trans-
form spectrometer (ACE-FTS) and imagers, *J. Quant. Spectrosc. Ra.*, 247, 106 939, <https://doi.org/10.1016/j.jqsrt.2020.106939>, 2020.
- Bourassa, A. E., Degenstein, D. A., Randel, W. J., Zawodny, J. M., Kyrölä, E., McLinden, C. A., Sioris, C. E., and Roth, C. Z.: Trends
840 in stratospheric ozone derived from merged SAGE II and Odin-OSIRIS satellite observations, *Atmos. Chem. Phys.*, 14, 6983–6994,
<https://doi.org/10.5194/acp-14-6983-2014>, 2014.
- Bourassa, A. E., Roth, C. Z., Zawada, D. J., Rieger, L. A., McLinden, C. A., and Degenstein, D. A.: Drift-corrected Odin-OSIRIS ozone
product: Algorithm and updated stratospheric ozone trends, *Atmos. Meas. Tech.*, 11, 489–498, <https://doi.org/10.5194/amt-11-489-2018>,
2018.
- 845 Brasseur, G. P. and Solomon, S.: *Aeronomy of the middle atmosphere: Chemistry and physics of the stratosphere and mesosphere*, Springer
Netherlands, Dordrecht, Great Britain, 3rd edn., 2005.
- Butchart, N.: The Brewer-Dobson circulation, *Rev. Geophys.*, 52, 157–184, <https://doi.org/10.1002/2013RG000448>, 2014.
- Butchart, N. and Remsberg, E. E.: The area of the stratospheric polar vortex as a diagnostic for tracer transport on an isentropic surface, *J.*
Atmos. Sci., 43, 1319–1339, [https://doi.org/10.1175/1520-0469\(1986\)043<1319:TAOTSP>2.0.CO;2](https://doi.org/10.1175/1520-0469(1986)043<1319:TAOTSP>2.0.CO;2), 1986.



- 850 Davis, S., Rosenlof, K., Hassler, B., Hurst, D., Read, W., Vömel, H., Selkirk, H., Fujiwara, M., and Damadeo, R.: The Stratospheric Water and Ozone Satellite Homogenized (SWOOSH) database: A long-term database for climate studies, *Earth Syst. Sci. Data*, 8, 461–490, <https://doi.org/10.5194/essd-8-461-2016>, 2016.
- Davis, S. M., Damadeo, R., Flittner, D., Rosenlof, K. H., Park, M., Randel, W. J., Hall, E. G., Huber, D., Hurst, D. F., Jordan, A. F., Kizer, S., Millan, L. F., Selkirk, H., Taha, G., Walker, K. A., and Vömel, H.: Validation of SAGE III/ISS Solar Water Vapor Data With Correlative
855 Satellite and Balloon-Borne Measurements, *J. Geophys. Res.: Atmos.*, 126, e2020JD033 803, <https://doi.org/10.1029/2020JD033803>, 2021.
- de Grandpré, J., Beagley, S. R., Fomichev, V. I., Griffioen, E., McConnell, J. C., Medvedev, A. S., and Shepherd, T. G.: Ozone climatology using interactive chemistry: Results from the Canadian Middle Atmosphere Model, *J. Geophys. Res.: Atmos.*, 105, 26 475–26 491, <https://doi.org/10.1029/2000JD900427>, 2000.
- 860 Degenstein, D. A., Bourassa, A. E., Roth, C. Z., and Llewellyn, E. J.: Limb scatter ozone retrieval from 10 to 60 km using a multiplicative algebraic reconstruction technique, *Atmos. Chem. Phys.*, 9, 6521–6529, <https://doi.org/10.5194/acp-9-6521-2009>, 2009.
- Eckstein, J., Ruhnke, R., Zahn, A., Neumaier, M., Kirner, O., and Braesicke, P.: An assessment of the climatological representativeness of IAGOS-CARIBIC trace gas measurements using EMAC model simulations, *Atmos. Chem. Phys.*, 17, 2775–2794, <https://doi.org/10.5194/acp-17-2775-2017>, 2017.
- 865 Fernando, A. M., Bernath, P. F., and Boone, C. D.: Stratospheric and mesospheric H₂O and CH₄ trends from the ACE satellite mission, *J. Quant. Spectrosc. Ra.*, 255, 107 268, <https://doi.org/10.1016/j.jqsrt.2020.107268>, 2020.
- Forster, P. M. d. F. and Shine, K. P.: Assessing the climate impact of trends in stratospheric water vapor, *Geophys. Res. Lett.*, 29, 1086, <https://doi.org/10.1029/2001GL013909>, 2002.
- Forster, P. M. F. and Shine, K. P.: Radiative forcing and temperature trends from stratospheric ozone changes, *J. Geophys. Res.: Atmos.*, 102,
870 10 841–10 855, <https://doi.org/10.1029/96JD03510>, 1997.
- Gelaro, R., McCarty, W., Suárez, M. J., Todling, R., Molod, A., Takacs, L., Randles, C. A., Darmenov, A., Bosilovich, M. G., Reichle, R., Wargan, K., Coy, L., Cullather, R., Draper, C., Akella, S., Buchard, V., Conaty, A., da Silva, A. M., Gu, W., Kim, G.-K., Koster, R., Lucchesi, R., Merkova, D., Nielsen, J. E., Partyka, G., Pawson, S., Putman, W., Rienecker, M., Schubert, S. D., Sienkiewicz, M., and Zhao, B.: The Modern-Era Retrospective Analysis for Research and Applications, version 2 (MERRA-2), *J. Climate*, 30, 5419–5454,
875 <https://doi.org/10.1175/JCLI-D-16-0758.1>, 2017.
- Gottelman, A., Hoor, P., Pan, L. L., Randel, W. J., Hegglin, M. I., and Birner, T.: The extratropical upper troposphere and lower stratosphere, *Rev. Geophys.*, 49, 3, <https://doi.org/10.1029/2011RG000355>, 2011.
- Haley, C. S., Brohede, S. M., Sioris, C. E., Griffioen, E., Murtagh, D. P., McDade, I. C., Eriksson, P., Llewellyn, E. J., Bazureau, A., and Goutail, F.: Retrieval of stratospheric O₃ and NO₂ profiles from Odin Optical Spectrograph and Infrared Imager System (OSIRIS) limb-scattered sunlight measurements, *J. Geophys. Res.: Atmos.*, 109, D16 303, <https://doi.org/10.1029/2004JD004588>, 2004.
- 880 Hegglin, M. I., Brunner, D., Peter, T., Hoor, P., Fischer, H., Staehelin, J., Krebsbach, M., Schiller, C., Parchatka, U., and Weers, U.: Measurements of NO, NO_y, N₂O, and O₃ during SPURT: Implications for transport and chemistry in the lowermost stratosphere, *Atmos. Chem. Phys.*, 6, 1331–1350, <https://doi.org/10.5194/acp-6-1331-2006>, 2006.
- Hegglin, M. I., Boone, C. D., Manney, G. L., Shepherd, T. G., Walker, K. A., Bernath, P. F., Daffer, W. H., Hoor, P., and Schiller, C.: Validation
885 of ACE-FTS satellite data in the upper troposphere/lower stratosphere (UTLS) using non-coincident measurements, *Atmos. Chem. Phys.*, 8, 1483–1499, <https://doi.org/10.5194/acp-8-1483-2008>, 2008.



- Hegglin, M. I., Gettelman, A., Hoor, P., Krichevsky, R., Manney, G. L., Pan, L. L., Son, S.-W., Stiller, G., Tilmes, S., Walker, K. A., Eyring, V., Shepherd, T. G., Waugh, D., Akiyoshi, H., Añel, J. A., Austin, J., Baumgaertner, A., Bekki, S., Braesicke, P., Brühl, C., Butchart, N., Chipperfield, M., Dameris, M., Dhomse, S., Frith, S., Garny, H., Hardiman, S. C., Jöckel, P., Kinnison, D. E., Lamarque, J. F., Mancini, E., Michou, M., Morgenstern, O., Nakamura, T., Olivié, D., Pawson, S., Pitari, G., Plummer, D. A., Pyle, J. A., Rozanov, E., Scinocca, J. F., Shibata, K., Smale, D., Teyssède, H., Tian, W., and Yamashita, Y.: Multimodel assessment of the upper troposphere and lower stratosphere: Extratropics, *J. Geophys. Res.: Atmos.*, 115, D00M09, <https://doi.org/10.1029/2010JD013884>, 2010.
- Hegglin, M. I., Tegtmeier, S., Anderson, J., Bourassa, A. E., Brohede, S., Degenstein, D., Froidevaux, L., Funke, B., Gille, J., Kasai, Y., Kyrölä, E. T., Lumpe, J., Murtagh, D., Neu, J. L., Pérot, K., Remsberg, E. E., Rozanov, A., Toohey, M., Urban, J., von Clarmann, T., Walker, K. A., Wang, H.-J., Arosio, C., Damadeo, R., Fuller, R. A., Lingenfelter, G., McLinden, C., Pendlebury, D., Roth, C., Ryan, N. J., Sioris, C., Smith, L., and Weigel, K.: Overview and update of the SPARC Data Initiative: comparison of stratospheric composition measurements from satellite limb sounders, *Earth Syst. Sci. Data*, 13, 1855–1903, <https://doi.org/10.5194/essd-13-1855-2021>, 2021.
- Holton, J. R., Haynes, P. H., McIntyre, M. E., Douglass, A. R., Rood, R. B., and Pfister, L.: Stratosphere-troposphere exchange, *Rev. Geophys.*, 33, 403–439, <https://doi.org/10.1029/95RG02097>, 1995.
- Hoor, P., Fischer, H., Lange, L., Lelieveld, J., and Brunner, D.: Seasonal variations of a mixing layer in the lowermost stratosphere as identified by the CO-O₃ correlation from in situ measurements, *J. Geophys. Res.: Atmos.*, 107, 4044, <https://doi.org/10.1029/2000JD000289>, 2002.
- Hoor, P., Gurk, C., Brunner, D., Hegglin, M. I., Wernli, H., and Fischer, H.: Seasonality and extent of extratropical TST derived from in-situ CO measurements during SPURT, *Atmos. Chem. Phys.*, 4, 1427–1442, <https://doi.org/10.5194/acp-4-1427-2004>, 2004.
- Hoor, P., Wernli, H., Hegglin, M. I., and Bönisch, H.: Transport timescales and tracer properties in the extratropical UTLS, *Atmos. Chem. Phys.*, 10, 7929–7944, <https://doi.org/10.5194/acp-10-7929-2010>, 2010.
- Hubert, D., Lambert, J.-C., Verhoelst, T., Granville, J., Keppens, A., Baray, J.-L., Bourassa, A. E., Cortesi, U., Degenstein, D. A., Froidevaux, L., Godin-Beekmann, S., Hoppel, K. W., Johnson, B. J., Kyrölä, E., Leblanc, T., Lichtenberg, G., Marchand, M., McElroy, C. T., Murtagh, D., Nakane, H., Portafaix, T., Querel, R., Russell III, J. M., Salvador, J., Smit, H. G. J., Stebel, K., Steinbrecht, W., Strawbridge, K. B., Stübi, R., Swart, D. P. J., Taha, G., Tarasick, D. W., Thompson, A. M., Urban, J., van Gijssel, J. A. E., Van Malderen, R., von der Gathen, P., Walker, K. A., Wolfram, E., and Zawodny, J. M.: Ground-based assessment of the bias and long-term stability of 14 limb and occultation ozone profile data records, *Atmos. Meas. Tech.*, 9, 2497–2534, <https://doi.org/10.5194/amt-9-2497-2016>, 2016.
- Hurst, D. F., Oltmans, S. J., Vömel, H., Rosenlof, K. H., Davis, S. M., Ray, E. A., Hall, E. G., and Jordan, A. F.: Stratospheric water vapor trends over Boulder, Colorado: Analysis of the 30 year Boulder record, *J. Geophys. Res.: Atmos.*, 116, D02306, <https://doi.org/10.1029/2010JD015065>, 2011.
- Jones, A., Walker, K. A., Jin, J. J., Taylor, J. R., Boone, C. D., Bernath, P. F., Brohede, S., Manney, G. L., McLeod, S., Hughes, R., and Daffer, W. H.: Technical Note: A trace gas climatology derived from the Atmospheric Chemistry Experiment Fourier Transform Spectrometer (ACE-FTS) data set, *Atmos. Chem. Phys.*, 12, 5207–5220, <https://doi.org/10.5194/acp-12-5207-2012>, 2012.
- Jonsson, A. I., de Grandpré, J., Fomichev, V. I., McConnell, J. C., and Beagley, S. R.: Doubled CO₂-induced cooling in the middle atmosphere: Photochemical analysis of the ozone radiative feedback, *J. Geophys. Res.: Atmos.*, 109, D24103, <https://doi.org/10.1029/2004JD005093>, 2004.
- Kar, J., McElroy, C. T., Drummond, J. R., Zou, J., Nichitiu, F., Walker, K. A., Randall, C. E., Nowlan, C. R., Dufour, D. G., Boone, C. D., Bernath, P. F., Treppe, C. R., Thomason, L. W., and McLinden, C.: Initial comparison of ozone and NO₂ profiles from ACE-MAESTRO with balloon and satellite data, *J. Geophys. Res.: Atmos.*, 112, D16, <https://doi.org/10.1029/2006JD008242>, 2007.



- Kolonjari, F., Plummer, D. A., Walker, K. A., Boone, C. D., Elkins, J. W., Hegglin, M. I., Manney, G. L., Moore, F. L., Pendlebury, D., Ray,
925 E. A., Rosenlof, K. H., and Stiller, G. P.: Assessing stratospheric transport in the CMAM30 simulations using ACE-FTS measurements,
Atmos. Chem. Phys., 18, 6801–6828, <https://doi.org/10.5194/acp-18-6801-2018>, 2018.
- Koo, J.-H., Walker, K. A., Jones, A., Sheese, P. E., Boone, C. D., Bernath, P. F., and Manney, G. L.: Global climatology based on the ACE-
FTS version 3.5 dataset: Addition of mesospheric levels and carbon-containing species in the UTLS, *J. Quant. Spectrosc. Ra.*, 186, 52–62,
<https://doi.org/10.1016/j.jqsrt.2016.07.003>, 2017.
- 930 Kunkel, D., Hoor, P., Petropavlovskikh, I., and Manney, G.: Report on the first SPARC OCTAV-UTLS meeting, Boulder, CO, USA, 18–20
July 2017, SPARC Newsletter, No. 50, 10–13, www.sparc-climate.org/publications/newsletter, 2018.
- Kunz, A., Schiller, C., Rohrer, F., Smit, H. G. J., Nedelec, P., and Spelten, N.: Statistical analysis of water vapour and ozone in the UT/LS
observed during SPURT and MOZAIC, *Atmos. Chem. Phys.*, 8, 6603–6615, <https://doi.org/10.5194/acp-8-6603-2008>, 2008.
- Kunz, A., Pan, L. L., Konopka, P., Kinnison, D. E., and Tilmes, S.: Chemical and dynamical discontinuity at the extratropical tropopause
935 based on START08 and WACCM analyses, *J. Geophys. Res.: Atmos.*, 116, D24 302, <https://doi.org/10.1029/2011JD016686>, 2011.
- Lacis, A. A., Wuebbles, D. J., and Logan, J. A.: Radiative forcing of climate by changes in the vertical distribution of ozone, *J. Geophys.
Res.: Atmos.*, 95, 9971–9981, <https://doi.org/10.1029/JD095iD07p09971>, 1990.
- Lelieveld, J. and Dentener, F. J.: What controls tropospheric ozone?, *J. Geophys. Res.: Atmos.*, 105, 3531–3551,
<https://doi.org/10.1029/1999JD901011>, 2000.
- 940 Lin, P. and Fu, Q.: Changes in various branches of the Brewer–Dobson circulation from an ensemble of chemistry climate models, *J. Geophys.
Res.: Atmos.*, 118, 73–84, <https://doi.org/10.1029/2012JD018813>, 2013.
- Llewellyn, E. J., Lloyd, N. D., Degenstein, D. A., Gattinger, R. L., Petelina, S. V., Bourassa, A. E., Wiensz, J. T., Ivanov, E. V., McDade,
I. C., Solheim, B. H., McConnell, J. C., Haley, C. S., von Savigny, C., Sioris, C. E., McLinden, C. A., Griffioen, E., Kaminski, J., Evans,
W. F. J., Puckrin, E., Strong, K., Wehrle, V., Hum, R. H., Kendall, D. J. W., Matsushita, J., Murtagh, D. P., Brohede, S., Stegman, J., Witt,
945 G., Barnes, G., Payne, W. F., Piché, L., Smith, K., Warshaw, G., Deslauniers, D.-L., Marchand, P., Richardson, E. H., King, R. A., Wevers,
I., McCreath, W., Kyrölä, E., Oikarinen, L., Leppelmeier, G. W., Auvinen, H., Mégie, G., Hauchecorne, A., Lefèvre, F., de La Nöe, J.,
Ricaud, P., Frisk, U., Sjöberg, F., von Schéele, F., and Nordh, L.: The OSIRIS instrument on the Odin spacecraft, *Can. J. Phys.*, 82,
411–422, <https://doi.org/10.1139/p04-005>, 2004.
- Lossow, S., Khosrawi, F., Kiefer, M., Walker, K. A., Bertaux, J.-L., Blanot, L., Russell, J. M., Remsberg, E. E., Gille, J. C., Sugita, T., Sioris,
950 C. E., Dinelli, B. M., Papandrea, E., Raspollini, P., García-Comas, M., Stiller, G. P., von Clarmann, T., Dudhia, A., Read, W. G., Nedoluha,
G. E., Damadeo, R. P., Zawodny, J. M., Weigel, K., Rozanov, A., Azam, F., Bramstedt, K., Noël, S., Burrows, J. P., Sagawa, H., Kasai, Y.,
Urban, J., Eriksson, P., Murtagh, D. P., Hervig, M. E., Högberg, C., Hurst, D. F., and Rosenlof, K. H.: The SPARC water vapour assessment
II: Profile-to-profile comparisons of stratospheric and lower mesospheric water vapour data sets obtained from satellites, *Atmos. Meas.
Tech.*, 12, 2693–2732, <https://doi.org/10.5194/amt-12-2693-2019>, 2019.
- 955 Manney, G. L. and Hegglin, M. I.: Seasonal and regional variations of long-term changes in upper-tropospheric jets from reanalyses, *J.
Climate*, 31, 423–448, <https://doi.org/10.1175/JCLI-D-17-0303.1>, 2018.
- Manney, G. L., Daffer, W. H., Zawodny, J. M., Bernath, P. F., Hoppel, K. W., Walker, K. A., Knosp, B. W., Boone, C., Remsberg, E. E.,
Santee, M. L., Harvey, V. L., Pawson, S., Jackson, D. R., Deaver, L., McElroy, C. T., McLinden, C. A., Drummond, J. R., Pumphrey,
H. C., Lambert, A., Schwartz, M. J., Froidevaux, L., McLeod, S., Takacs, L. L., Suarez, M. J., Trepte, C. R., Cuddy, D. C., Livesey, N. J.,
960 Harwood, R. S., and Waters, J. W.: Solar occultation satellite data and derived meteorological products: Sampling issues and comparisons
with Aura Microwave Limb Sounder, *J. Geophys. Res.: Atmos.*, 112, D24S50, <https://doi.org/10.1029/2007JD008709>, 2007.



- Manney, G. L., Hegglin, M. I., Daffer, W. H., Santee, M. L., Ray, E. A., Pawson, S., Schwartz, M. J., Boone, C. D., Froidevaux, L., Livesey, N. J., Read, W. G., and Walker, K. A.: Jet characterization in the upper troposphere/lower stratosphere (UTLS): applications to climatology and transport studies, *Atmos. Chem. Phys.*, 11, 6115–6137, <https://doi.org/10.5194/acp-11-6115-2011>, 2011.
- 965 Manney, G. L., Hegglin, M. I., Daffer, W. H., Schwartz, M. J., Santee, M. L., and Pawson, S.: Climatology of upper tropospheric–lower stratospheric (UTLS) jets and tropopauses in MERRA, *J. Climate*, 27, 3248–3271, <https://doi.org/10.1175/JCLI-D-13-00243.1>, 2014.
- Manney, G. L., Hegglin, M. I., Lawrence, Z. D., Wargan, K., Millán, L. F., Schwartz, M. J., Santee, M. L., Lambert, A., Pawson, S., Knosp, B. W., Fuller, R. A., and Daffer, W. H.: Reanalysis comparisons of upper tropospheric–lower stratospheric jets and multiple tropopauses, *Atmos. Chem. Phys.*, 17, 11 541–11 566, <https://doi.org/10.5194/acp-17-11541-2017>, 2017.
- 970 McCormick, M. P., Lei, L., Hill, M. T., Anderson, J., Querel, R., and Steinbrecht, W.: Early results and validation of SAGE III-ISS ozone profile measurements from onboard the International Space Station, *Atmos. Meas. Tech.*, 13, 1287–1297, <https://doi.org/10.5194/amt-13-1287-2020>, 2020.
- McElroy, C. T., Nowlan, C. R., Drummond, J. R., Bernath, P. F., Barton, D. V., Dufour, D. G., Midwinter, C., Hall, R. B., Ogyu, A., Ullberg, A., Wardle, D. I., Kar, J., Zou, J., Nichitiu, F., Boone, C. D., Walker, K. A., and Rowlands, N.: The ACE-MAESTRO instrument on SCISAT: Description, performance, and preliminary results, *Appl. Optics.*, 46, 4341–4356, <https://doi.org/10.1364/AO.46.004341>, 2007.
- McLandress, C., Scinocca, J. F., Shepherd, T. G., Reader, M. C., and Manney, G. L.: Dynamical control of the mesosphere by orographic and non-orographic gravity wave drag during the extended northern winters of 2006 and 2009, *J. Atmos. Sci.*, 70, 2152–2169, <https://doi.org/10.1175/JAS-D-12-0297.1>, 2013.
- McLandress, C., Plummer, D. A., and Shepherd, T. G.: Technical Note: A simple procedure for removing temporal discontinuities in ERA-Interim upper stratospheric temperatures for use in nudged chemistry-climate model simulations, *Atmos. Chem. Phys.*, 14, 1547–1555, <https://doi.org/10.5194/acp-14-1547-2014>, 2014.
- 980 Millán, L. F., Livesey, N. J., Santee, M. L., Neu, J. L., Manney, G. L., and Fuller, R. A.: Case studies of the impact of orbital sampling on stratospheric trend detection and derivation of tropical vertical velocities: solar occultation vs. limb emission sounding, *Atmos. Chem. Phys.*, 16, 11 521–11 534, <https://doi.org/10.5194/acp-16-11521-2016>, 2016.
- 985 Murtagh, D., Frisk, U., Merino, F., Ridal, M., Jonsson, A., Stegman, J., Witt, G., Eriksson, P., Jiménez, C., Megie, G., de la Noë, J., Ricaud, P., Baron, P., Pardo, J. R., Hauchcorne, A., Llewellyn, E. J., Degenstein, D. A., Gattinger, R. L., Lloyd, N. D., Evans, W. F. J., McDade, I. C., Haley, C. S., Sioris, C., von Savigny, C., Solheim, B. H., McConnell, J. C., Strong, K., Richardson, E. H., Leppelmeier, G. W., Kyrölä, E., Auvinen, H., and Oikarinen, L.: An overview of the Odin atmospheric mission, *Can. J. Phys.*, 80, 309–319, <https://doi.org/10.1139/p01-157>, 2002.
- 990 Neu, J. L., Hegglin, M. I., Tegtmeier, S., Bourassa, A., Degenstein, D., Froidevaux, L., Fuller, R., Funke, B., Gille, J., Jones, A., Rozanov, A., Toohey, M., von Clarmann, T., Walker, K. A., and Worden, J. R.: The SPARC Data Initiative: Comparison of upper troposphere/lower stratosphere ozone climatologies from limb-viewing instruments and the nadir-viewing Tropospheric Emission Spectrometer, *J. Geophys. Res.: Atmos.*, 119, 6971–6990, <https://doi.org/10.1002/2013JD020822>, 2014.
- Noël, S., Weigel, K., Bramstedt, K., Rozanov, A., Weber, M., Bovensmann, H., and Burrows, J. P.: Water vapour and methane coupling in the stratosphere observed using SCIAMACHY solar occultation measurements, *Atmos. Chem. Phys.*, 18, 4463–4476, <https://doi.org/10.5194/acp-18-4463-2018>, 2018.
- Pan, L. L., Randel, W. J., Gary, B. L., Mahoney, M. J., and Hints, E. J.: Definitions and sharpness of the extratropical tropopause: A trace gas perspective, *J. Geophys. Res.: Atmos.*, 109, D23 103, <https://doi.org/10.1029/2004JD004982>, 2004.



- 1000 Pan, L. L., Kunz, A., Homeyer, C. R., Munchak, L. A., Kinnison, D. E., and Tilmes, S.: Commentary on using equivalent latitude in the upper troposphere and lower stratosphere, *Atmos. Chem. Phys.*, 12, 9187–9199, <https://doi.org/10.5194/acp-12-9187-2012>, 2012.
- Pendlebury, D., Plummer, D., Scinocca, J., Sheese, P. E., Strong, K., Walker, K. A., and Degenstein, D.: Comparison of the CMAM30 data set with ACE-FTS and OSIRIS: Polar regions, *Atmos. Chem. Phys.*, 15, 12465–12485, <https://doi.org/10.5194/acp-15-12465-2015>, 2015.
- Plumb, R. A.: Stratospheric transport, *J. Meteorol. Soc. Jpn.*, 80, 793–809, <https://doi.org/10.2151/jmsj.80.793>, 2002.
- 1005 Randel, W. J., Wu, F., Russell, J. M., Roche, A., and Waters, J. W.: Seasonal Cycles and QBO variations in stratospheric CH₄ and H₂O observed in UARS HALOE Data, *J. Atmos. Sci.*, 55, 163–185, <https://doi.org/10.1175/1520-0469>, 1998.
- Randel, W. J., Wu, F., Vömel, H., Nedoluha, G. E., and Forster, P.: Decreases in stratospheric water vapor after 2001: Links to changes in the tropical tropopause and the Brewer-Dobson circulation, *J. Geophys. Res.: Atmos.*, 111, <https://doi.org/10.1029/2005JD006744>, 2006.
- Riese, M., Ploeger, F., Rap, A., Vogel, B., Konopka, P., Dameris, M., and Forster, P.: Impact of uncertainties in atmospheric mixing on simulated UTLS composition and related radiative effects, *J. Geophys. Res.: Atmos.*, 117, D16305, <https://doi.org/10.1029/2012JD017751>,
1010 2012.
- Roelofs, G.-J. and Lelieveld, J.: Model study of the influence of cross-tropopause O₃ transports on tropospheric O₃ levels, *Tellus B*, 49, 38–55, <https://doi.org/10.3402/tellusb.v49i1.15949>, 1997.
- Scinocca, J. F., McFarlane, N. A., Lazare, M., Li, J., and Plummer, D.: Technical Note: The CCCma third generation AGCM and its extension into the middle atmosphere, *Atmos. Chem. Phys.*, 8, 7055–7074, <https://doi.org/10.5194/acp-8-7055-2008>, 2008.
- 1015 Sheese, P. E., Boone, C. D., and Walker, K. A.: Detecting physically unrealistic outliers in ACE-FTS atmospheric measurements, *Atmos. Meas. Tech.*, 8, 741–750, <https://doi.org/10.5194/amt-8-741-2015>, 2015.
- Sheese, P. E., Walker, K. A., Boone, C. D., Bernath, P. F., Froidevaux, L., Funke, B., Raspollini, P., and von Clarmann, T.: ACE-FTS ozone, water vapour, nitrous oxide, nitric acid, and carbon monoxide profile comparisons with MIPAS and MLS, *J. Quant. Spectrosc. Ra.*, 186, 63–80, <https://doi.org/10.1016/j.jqsrt.2016.06.026>, 2017.
- 1020 Sheese, P. E., Walker, K. A., Boone, C. D., Degenstein, D. A., Kolonjari, F., Plummer, D., Kinnison, D. E., Jöckel, P., and von Clarmann, T.: Model estimations of geophysical variability between satellite measurements of ozone profiles, *Atmos. Meas. Tech.*, 14, 1425–1438, <https://doi.org/10.5194/amt-14-1425-2021>, 2021.
- Sheese, P. E., Walker, K. A., Boone, C. D., Bourassa, A. E., Degenstein, D. A., Froidevaux, L., McElroy, C. T., Murtagh, D., Russell III, J. M., and Zou, J.: Assessment of the quality of ACE-FTS stratospheric ozone data, *Atmos. Meas. Tech.*, 15, 1233–1249,
1025 <https://doi.org/10.5194/amt-15-1233-2022>, 2022.
- Shepherd, T., Plummer, D., Scinocca, J., Hegglin, M., Fioletov, V., Reader, M., Remsberg, E., Clarmann, T., and Wang, H.: Reconciliation of halogen-induced ozone loss with the total-column ozone record, *Nat. Geosci.*, 7, 443–449, <https://doi.org/10.1038/ngeo2155>, 2014.
- Sioris, C. E., Zou, J., McElroy, C. T., McLinden, C. A., and Vömel, H.: High vertical resolution water vapour profiles in the upper troposphere and lower stratosphere retrieved from MAESTRO solar occultation spectra, *Adv. Space. Res.*, 46, 642–650,
1030 <https://doi.org/10.1016/j.asr.2010.04.040>, 2010.
- Sioris, C. E., McLinden, C. A., Fioletov, V. E., Adams, C., Zawodny, J. M., Bourassa, A. E., Roth, C. Z., and Degenstein, D. A.: Trend and variability in ozone in the tropical lower stratosphere over 2.5 solar cycles observed by SAGE II and OSIRIS, *Atmos. Chem. Phys.*, 14, 3479–3496, <https://doi.org/10.5194/acp-14-3479-2014>, 2014.
- Sioris, C. E., Zou, J., Plummer, D. A., Boone, C. D., McElroy, C. T., Sheese, P. E., Moeni, O., and Bernath, P. F.: Upper tropospheric water vapour variability at high latitudes – Part 1: Influence of the annular modes, *Atmos. Chem. Phys.*, 16, 3265–3278,
1035 <https://doi.org/10.5194/acp-16-3265-2016>, 2016.



- Sofieva, V. F., Tamminen, J., Kyrölä, E., Mielonen, T., Veefkind, P., Hassler, B., and Bodeker, G. E.: A novel tropopause-related climatology of ozone profiles, *Atmos. Chem. Phys.*, 14, 283–299, <https://doi.org/10.5194/acp-14-283-2014>, 2014.
- 1040 Solomon, S., Rosenlof, K. H., Portmann, R. W., Daniel, J. S., Davis, S. M., Sanford, T. J., and Plattner, G.-K.: Contributions of stratospheric water vapor to decadal changes in the rate of global warming, *Science*, 327, 1219–1223, <https://doi.org/10.1126/science.1182488>, 2010.
- SPARC-CCMVal: The SPARC (Stratospheric Processes And their Role in Climate): Report on the evaluation of chemistry-climate models, SPARC Report No. 5, WCRP-30/2010, WMO/TD – No. 40, <https://www.sparc-climate.org/publications/sparc-reports/sparc-report-no-5/>, last access: 23 September 2021, 2010.
- SPARC-DI: The SPARC (Stratospheric Processes And their Role in Climate) Data Initiative: Assessment of stratospheric trace gas and aerosol climatologies from satellite limb sounders, SPARC Report No. 8, WCRP-05/2017, <https://doi.org/10.3929/ethz-a-010863911>, 2017.
- 1045 SPARC-LOTUS: The SPARC (Stratospheric Processes And their Role in Climate): Report on long-term ozone trends and uncertainties in the stratosphere, SPARC Report No. 9, GAW Report No. 241, WCRP-17/2018, <https://doi.org/10.17874/f899e57a20b>, 2019.
- Toohey, M. and von Clarmann, T.: Climatologies from satellite measurements: The impact of orbital sampling on the standard error of the mean, *Atmos. Meas. Tech.*, 6, 937–948, <https://doi.org/10.5194/amt-6-937-2013>, 2013.
- 1050 Toohey, M., Hegglin, M. I., Tegtmeier, S., Anderson, J., Añel, J. A., Bourassa, A., Brohede, S., Degenstein, D., Froidevaux, L., Fuller, R., Funke, B., Gille, J., Jones, A., Kasai, Y., Krüger, K., Kyrölä, E., Neu, J. L., Rozanov, A., Smith, L., Urban, J., von Clarmann, T., Walker, K. A., and Wang, R. H. J.: Characterizing sampling biases in the trace gas climatologies of the SPARC Data Initiative, *J. Geophys. Res.: Atmos.*, 118, 11 847–11 862, <https://doi.org/10.1002/jgrd.50874>, 2013.
- 1055 Vigouroux, C., De Mazière, M., Demoulin, P., Servais, C., Hase, F., Blumenstock, T., Kramer, I., Schneider, M., Mellqvist, J., Strandberg, A., Velasco, V., Notholt, J., Sussmann, R., Stremme, W., Rockmann, A., Gardiner, T., Coleman, M., and Woods, P.: Evaluation of tropospheric and stratospheric ozone trends over Western Europe from ground-based FTIR network observations, *Atmos. Chem. Phys.*, 8, 6865–6886, <https://doi.org/10.5194/acp-8-6865-2008>, 2008.
- Weaver, D., Strong, K., Walker, K. A., Sioris, C. E., Schneider, M., McElroy, C. T., Vömel, H., Sommer, M., Weigel, K., Rozanov, A., 1060 Burrows, J. P., Read, W. G., Fishbein, E., and Stiller, G.: Comparison of ground-based and satellite measurements of water vapour vertical profiles over Ellesmere Island, Nunavut, *Atmos. Meas. Tech.*, 12, 4039–4063, <https://doi.org/10.5194/amt-12-4039-2019>, 2019.
- Zahn, A., Christner, E., van Velthoven, P. F. J., Rauthe-Schöch, A., and Brenninkmeijer, C. A. M.: Processes controlling water vapor in the upper troposphere/lowermost stratosphere: An analysis of 8 years of monthly measurements by the IAGOS-CARIBIC observatory, *J. Geophys. Res.: Atmos.*, 119, 11 505–11 525, <https://doi.org/10.1002/2014JD021687>, 2014.